SIMULATION AND ANALYTICAL STUDY OF FIBER BREAKAGE OF LONG FIBER REINFORCED THERMOPLASTIC COMPOSITES IN INJECTION MOLDING

ADITYA SINGH CHAUHAN

TU Delft

Simulation and analytical study of fiber breakage of long fiber reinforced thermoplastic composites in injection molding

Thesis Report

to obtain the degree of Master of Science at Delft University of Technology

by

ADITYA SINGH CHAUHAN
Student Number: 5308984
Department of 3mE,
TU Delft, Delft, Netherlands.

Supervisors	Dr. A. Rezaei
	Prof. Dr. S.J. Picken
	Prof. Dr. M.A. Bessa
Thesis Committee	Dr. A. Rezaei
	Prof. Dr. S.J. Picken
	Prof. Dr. M.A. Bessa
	Prof. Dr. V. Popovich
	Prof. Dr. B. Caglar
Project Duration	March 1, 2022 - November 28, 2022

This work is performed in collaboration with Brightlands Materials Center (TNO), Geleen, Netherlands

ACKNOWLEDGEMENT

This thesis report is the encapsulation of the hard work which I carried over the past few months to find answers to some research questions which were posed with a very curious, hopeful and slightly naive brain. However, over the course of this period, the curiosity and hopefulness still remain, while the knowledge and confidence as a researcher has increased significantly. This growth would not have been possible without the constant guidance and support of Dr. Ali Rezaei, who provided me a wonderful opportunity to take part in this research topic at Brightlands Materials Center (TNO), Geleen. His constant presence and solutions to tackle obstacles were always a major help and provided the boost I needed to move forward. I would further like to thank Dr. Stephen Picken and Dr. Miguel Bessa for their support as academic supervisors to my project. Prof. Stephen has been really helpful in providing a much holistic approach to interpret the results and seek various paths leading to achieve a research objective. While Prof. Miguel has helped me understand the importance of a planned and radical approach towards research, and the edge which asking the right questions can provide.

The completion of this thesis also marks the end of my journey as the student of Delft University of Technology, which has provided me with more than two years of wonderful learning and growing experience. As a student, it has been a really enjoyable period where I have come across many amazing and interesting people, some of whom I have had the fortune to be friends with. I am grateful to them for their support and presence in need to make this period (including corona time) much colorful.

Finally I would like to thank my family, who have been just the best and always provided their unconditional love and support to make me reach this far.

Aditya Singh Chauhan
Delft, November 2022

ABSTRACT

The superior nature of long fiber reinforced thermoplastics (LFTs) in terms of properties such as specific modulus, strength and excellent impact resistance, along with their lightweight properties, ease of processability and recyclability make them one of the most competitive materials leading to their growth in various fields of applications.
With the growing rise of LFTs, the research on their mechanical properties and their processing has grown as well. Injection molding method has been one of the most widely applied production method for LFTs processing. Research has shown that the mechanical edge offered by the LFT products obtained from injection molding is dependent on the lengths of the fibers in the final product. This makes it important to understand the breakage of fibers during processing.
This work addresses the breakage of fiber in injection molding by conducting a thorough review of the industrial, experimental and theoretical research done in the field. Following this, simulation approach has been undertaken to understand the fiber breakage in geometries which represent slightly complex shapes as compared to the conventionally used shapes. Based on the theoretical research, the state-of-the-art models have been reviewed and compared in their ability to produce reliable fiber breakage results.
The results showed the influence of rheology and geometry on fiber breakage in simulations, where shear rates led to higher fiber breakage and increasing viscosity led to a slight reduction in breakage. Further, the simulation study provided inconsistent results with variation in geometry, and a need for further fine tuning of simulation parameters was observed. The theoretical models applied in the study gave reliable results in terms of the trends of the fiber breakage, with a novel model, called Bechara model, showing acceptable and more time efficient results, in comparison with the currently applied commercial model, Phelps model.

CONTENTS

List of Figures

LIST OF TABLES

NOMENCLATURE

FC	Fiber Concentration
FEM	Finite Element Method
FLD	Fiber Length Distribution
FO	Fiber Orientation
FRP	Fiber Reinforced Plastics
FRPC	Fiber Reinforce Polymer Composites
LFT	Long Fiber Thermoplastics
PDF	Probability Distribution Function
SFD	Schulz Flory Distribution
SFT	Short Fiber Thermoplastics

1

INTRODUCTION

Long fiber-reinforced thermoplastics (LFTs) are composite materials comprising of thermoplastic polymer material as a matrix and reinforcements of long discontinuous fibers. These composites can be characterised by considerable mechanical properties, excellent processability, low density, recyclability and infinite shelf life, to name a few [1]. Compared to short fiber reinforced composites (SFTs), LFTs offer superior mechanical properties like elastic modulus, strength and impact, whereas compared to continuous thermoplastics, they offer better processability (as shown in the Figure 1.1).

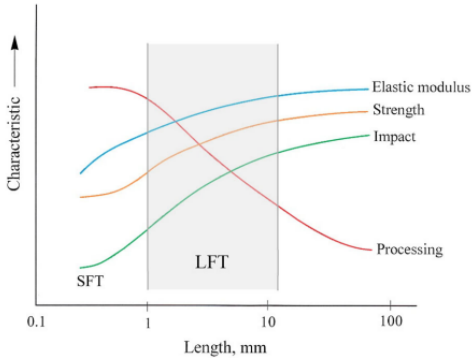

Figure 1.1: The effect of fiber lengths on the mechanical properties and the processability of the composites. The shaded area represents the LFTs, while area to the left and right of the shaded region indicates SFTs and continuous fibers, respectively. Reproduced from literature [1].

Owing to these superior properties and the general trend to push towards lightweight materials in aerospace and automotive industries, LFTs have found an increase in application in the various industrial sectors, causing its production to rise up drastically in the recent few decades ([1], [2]). As a consequence of this, injection molding process has

been widely applied to keep up with the demand and provide a reliable finalised product. The selection of injection molding among various processing techniques available depends on various factors such as type and nature of composite material, speed and ease of processing, and quantity of products to be formed. Based on these factors, injection molding offers a favourable choice. However, the mechanical advantages offered by different thermoplastic materials can be compromised during the processing stage, due to changes in the structure of the material. One of the major changes observed about the material is the fiber length of the composite fibers processed in production. The fiber breakage of the LFTs during production impacts severely the mechanical properties of the product. Various literature have emphasized on the correlation between the fiber lengths and the resulting mechanical properties ([3], [4]). As a result, controlling the conditions of processing technique is important to ensure the preservation of the fiber length, and in turn, the useful material properties.

This work is aimed at performing a thorough study about the fiber breakage in injection molding process and understand the factors that lead to fiber attrition in the processing. In this report, first chapter 2 provides a literature background covering the various materials which can be used for the production of the LFT composites, and the production processes commonly used. This is followed by the review of state of the art work currently conducted to address the fiber breakage in injection molding and relevant research associated to it. Following the literature review, the gaps and opportunities for further research are presented in the work, based on which research objectives are set for this thesis project. chapter 3 then covers the concerning methodology and work performed in this study to address the proposed research objectives. The results are then presented in the chapter 4 followed by the conclusions and future recommendations on this work, which are presented in chapter 5.

2

THEORETICAL BACKGROUND

2.1. MATERIALS

Polymeric products such as plastics have been in widespread use among various applications. They can primarily be classified into two major types: thermoplastics and thermosets ([5], [6]). Thermoplastics can undergo various heating and cooling cycles, becoming soft and hard again, making them suitable for recycling. Whereas thermosets retain their shape and structure, even at higher temperatures, and they cannot be remoulded once they melt [7]. This basic difference in the properties of the thermosets and thermoplastics resides in their atomic structural arrangement. While thermoplastics contain chains of carbon that work independently, thermosets possess a three-dimensional cross-linking between these chains, making them more resistant to deforming [5]. The schematics of these polymer types are shown in Figure 2.1.

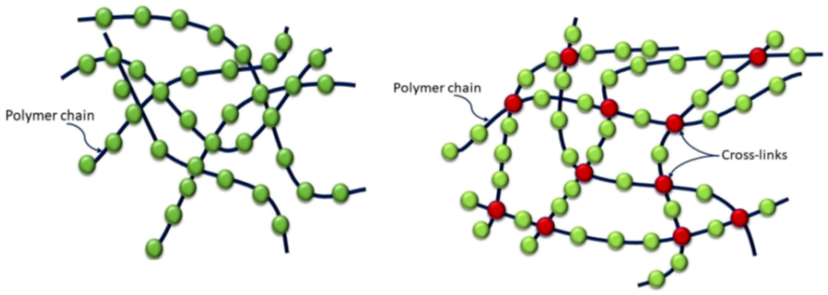

Figure 2.1: The schematics of thermoplastic and thermoset polymeric materials: (left) thermoplastics, with weak intermolecular forces between polymer chains; (right). Taken from literature [5].

Since composites consist of two or more distinct constituent materials, these polymers need to be combined with a different material to generate the composite. The polymeric constituents can be combined with fiber where fibers act as reinforcing phase for

mechanical properties and polymers act as binding phase. This provides with final product called fiber reinforced plastic (FRP) or fiber reinforced polymer composites (FRPC) [8]. Depending on the type of polymer, the two common FRPs are thermoplastic composites and thermosetting composites, with the distinction that thermoplastic composites can be remoulded in contrast to thermosets (as seen before). Due to their recyclability and ease of manufacturing, thermoplastic composites have emerged as competitor against thermoset composites, and appear as a better prospect with the concept of sustainability in mind. Further, Vaidya et al. [9] mentions some other advantages of thermoplastic composites over thermoset composites such as enhanced mechanical properties in terms of impact and abrasion, better adaptability to manufacturability, more environmental friendly nature, and recyclability.

2.1.1. MATERIAL CONSTITUENTS

The major components of fiber-reinforced composites are the matrix, the fibers, and the interphase between the two determining the strength of their bonding [10]. The mechanical, thermal and structural properties of the final composite products are influenced by the choice of these materials. These materials are discussed as follows:

MATRIX

The matrix is the base of the composite in which the fiber is added. The main purpose of the matrix is to act as a binding phase and provide structural integrity to the composite. Thermoplastic resin or matrix offers better impact resistance and higher toughness as compared to thermosetting resin [10]. This allows it to withstand extensive damage without cracking and failing. The material properties for few common resins are shown in the Table 2.1.

Table 2.1: Some common matrix polymers and their properties ([9]–[11]).

	Tensile modulus, GPa	Tensile strength (yield), MPa	Melting point, °C	Density,g/cm^3
Polypropylene -PP	1.35–1.70	28–39	134–165	0.89–0.91
Polyethylene-PE	0.15	10–18	104–113	0.918–0.919
Polyurethane - PU	0.028–0.72	5–28	220–230	1.15–1.25
Polyamides - PA	0.7–3.3	40–86	211–265	1.03–1.16
Polyether sulphone - PES	2.4–8.62	83–126	220	1.36–1.58

Few of the common resins are as follows:

Polypropylene (PP): It is a good solvent matrix with high toughness, reasonable stiffness, and good strength with relatively low melting point ([10] & [9]). It is commonly produced, for composites, with short and long fiber injection/extrusion/compression molding techniques [12].

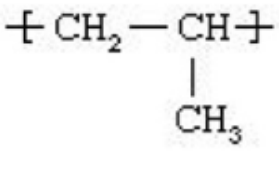

Figure 2.2: chemical structure of polypropylene. Reproduced from [10].

Polyethylene (PE): It is the most commonly used thermoplastic in the world due to high toughness, low electrical conductivity and chemically inert nature [10]. However, its applications are limited to temperature below 150°C [9].

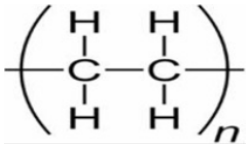

Figure 2.3: chemical structure of polyethylene. Reproduced from [10].

Polyurethane (PU): It behaves like an elastomer with high strain to fracture ratio, with durability and high toughness. It finds applications in paints, liquid coatings, elastic rubbers, foams etc. ([10] & [9]).

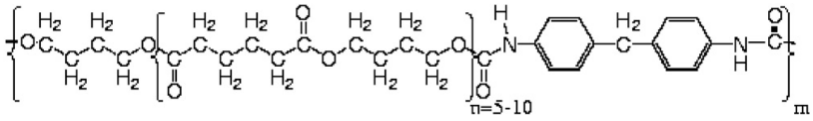

Figure 2.4: chemical structure of polyurethane. Reproduced from [10].

FIBERS

In a composite material, the fiber acts as the reinforcing material for bearing the loads and contributing towards the strength and stiffness of the composite [10] . Fibers tend to possess higher elastic modulus as compared to the matrices and show higher rigidity under loading conditions as well. This causes the interphase regions between the fibers and the matrix to be more prone to initial damage. The choice of fibers can be made between two major categories of fibers, synthetic or natural. While synthetic fibers, such as glass, carbon and aramid, have been more of the norm in the past few years ([13], [14]), natural fibers, such as jute and flax, have been gaining some ground in recent times as an alternative due to environmentally friendly properties with cheap price and good mechanical characteristics ([15], [16]). Some common reinforcing fibers along with their properties are shown in the Table 2.2:

Table 2.2: Mechanical and physical properties of some commonly available synthetic and natural fibers . Found in literature [9], [13], [17]–[26]. *Note: The properties are given in a range due to various types of fibers available of each kind based on the fiber weight*

Fibre	Young's Modulus (GPa)	Tensile strength (GPa)	Density (g/cm^3)
Glass	65-90	3-4	2.5
Carbon	250-500	2.5-4	1.6-2.0
Aramid (Kevlar)	80-125	2.8-3.5	1.46
Jute	13-26.5	393-800	1.3-1.49
Hemp	70	690	1.47

Some important **synthetic fibers** are mentioned as follows:
Glass fibers: They are widely used type of fibers with 93% of FRPs being reinforced with glass fibers. Printing boards, structural composites are some common products made from them [27]–[29]. Common type of glass fibers are E-glass fibers, which are the oldest and electrical grade, A and C-glass fibers, which are resistant to chemicals [11].
Carbon fibers: They provide the maximum specific strength and modulus with good thermal and electrical conductivities [24]. These properties make them ideal for use in the automobile, electronics and aerospace industries [25]. The strength of these fibers increases with increasing carbon content or degree of graphitization.
Aramid fibers (Kevlar): They contain a strong molecular structure, made of Poly-para-phenylene terepthalamide (PPTA). They are very commonly used in technologies like helicopter blades, ballistic armour, sporting goods etc [17]. They exhibit excellent properties at high temperatures and possess considerable tensile strength and modulus.

Some of the common **natural fibers** are as follows:
Jute: It is a soft and shiny plant fiber which can produce fibers of length ranging from 1-4 metres long. It is one of the strongest natural fiber with high tensile strength and low extensibility used for making cloth for wrapping bales of raw cotton, sacs and coarse cloth [30].
Hemp: It is one of the most widely used natural fiber as reinforcement in composites. It offers advantages over thermosets in terms of processing cost and design flexibility. It can be used for making products like guideposts, boats, furniture and loudspeakers etc. It also contain the potential to replace glass fibers for various applications [31].
After analysing the available options and considering the final application, a choice for the constituents for the final thermoset or thermoplastic composite can be made. In this work, the major focus has been made on thermoplastic composites as they offer certain properties of interest such as recyclability and ease of manufacturing, which are already discussed in the beginning of section 2.1. The excellent properties offered by the thermoplastic fiber reinforced composites (FRPs) at a much-reduced weight have boosted their use in different sectors. Sectors like defence, aerospace, marine, construction, and automobile, have been the few to realise the benefits of these composites over conventional metals [32].

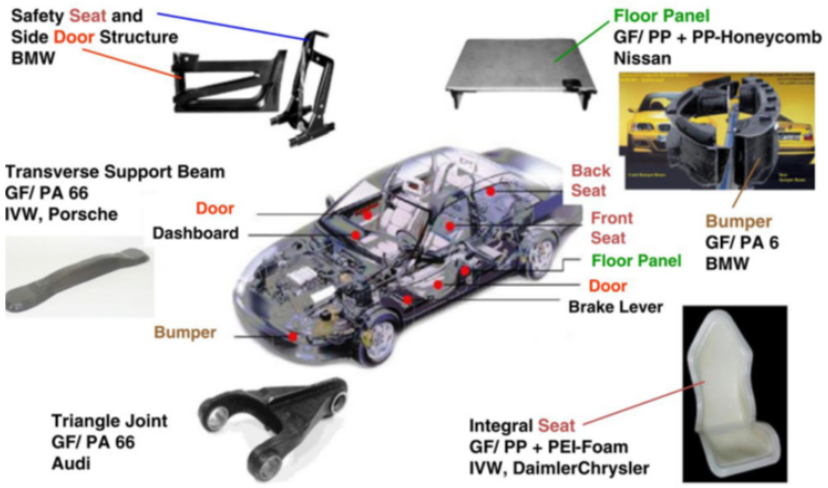

Figure 2.5: Common applications of FRPs in automobile structures. Reproduced from [10].

2.2. PROCESSES

Depending on the need for production, in terms of quantity, quality and costs, various production process can be proposed. Discussed ahead are the few of the common manufacturing technologies for thermoplastic FRPs.

2.2.1. AUTOCLAVE

An autoclave process is a method in which a large pressure vessel with an integrated heating facility, or an autoclave, is used to impregnate thermoplastic material and convert them into a finalised shape [8]. The process is relatively time consuming and cost intensive ([33], [34]). It is used to produce high performance parts with applications in aerospace, military and high-performance sports industries.

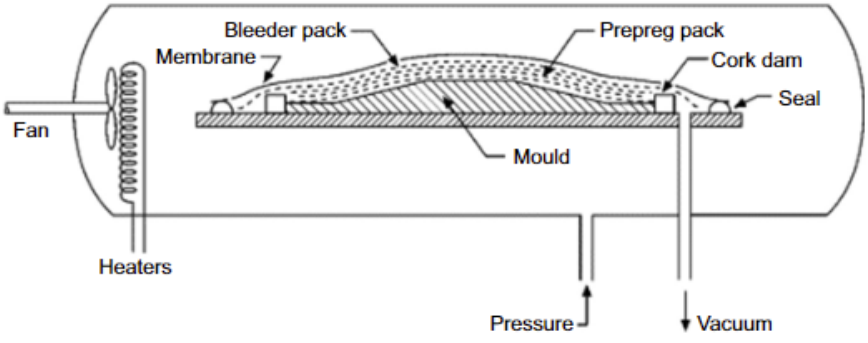

Figure 2.6: Schematic of autoclave process. Reproduced from [35].

2.2.2. COMPRESSION MOLDING

It is a highly automated and reproducible process with high dimensional accuracy. It provides products for applications in transportation, electrical appliances, construction, and sports. In this process polymer pellets are heated and converted into a melt which is compressed within a mold of desired shape, and finally cooled to solidify into the final shape. The only limitation to the compression molding is the complexity of the mold design itself ([8], [36]).

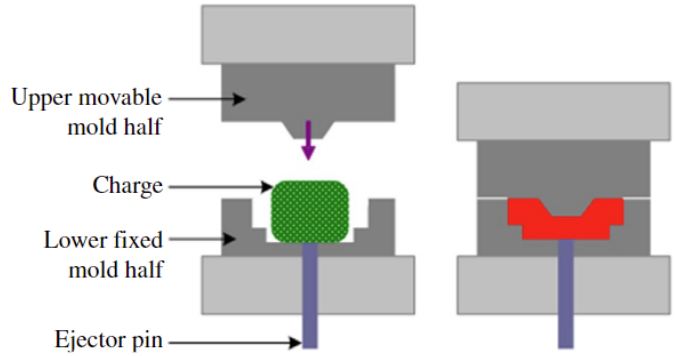

Figure 2.7: Schematic of compression molding. Reproduced from [37]

2.2.3. PULTRUSION

It is method of producing unidirectional fiber-reinforced profiles with constant cross sections [8]. It is characterised by high level of automation, low labour costs and high part quality making it favourable for mass production ([38], [39]).

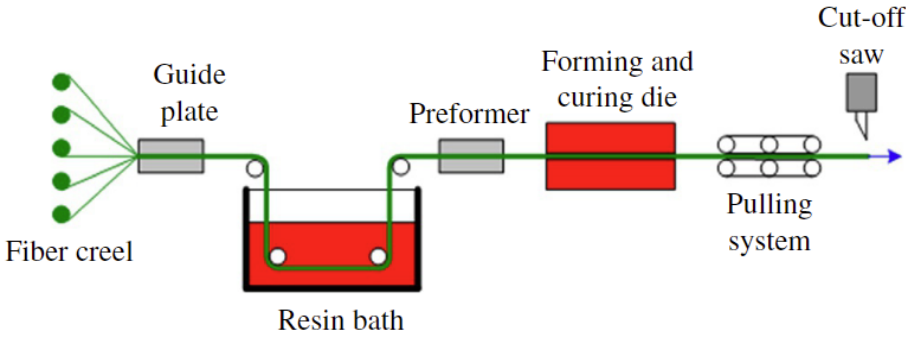

Figure 2.8: Schematic of pultrusion process. Reproduced from [37].

Apart from the common processes mentioned until here, this work focuses mainly on the injection molding process, which will be discussed in detail here on.

2.2.4. INJECTION MOLDING

Injection molding has been one of the most important polymer processing techniques for producing plastic composite parts made of thermoplastics, thermosets or elastomers. For commonly used composite materials, such as glass fibers, injection molding has the capability to produce near net shape articles with remarkable physical and mechanical properties [40].

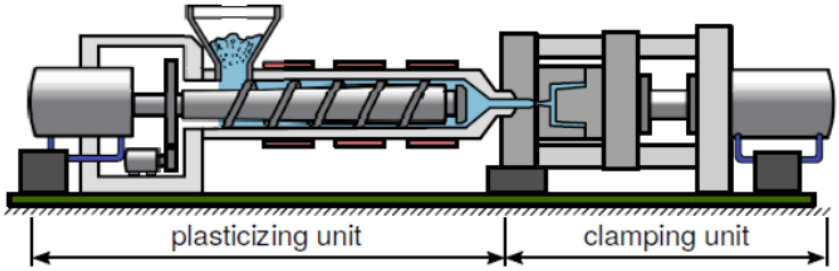

Figure 2.9: Schematic of injection molding. Reproduced from [41].

The modern injection molding techniques could be used to make parts ranging from 1 mg upto 100 kg [8]. The major advantage of injection molding resides in its ability to produce parts in high volume with less time making it suitable for applications in aerospace and automotive industry. While the advantage of an injection molding process involves extremely fast and automated production process with production of complex geometries, its disadvantage includes the fact that the cost of manufacturing the cavity molds are relatively high as compared to the actual process. As a consequence, it becomes important to prevent modifications in mold by ensuring an optimal design in the beginning of the molding process ([8], [41]).
The process of injection molding itself is relatively simple and straightforward. The injection molding setup can be subdivided into the two basic units, a plasticizing unit and the clamping unit (Figure 2.9). In the plasticizing unit, the main sections are the conveyor zone, transition zone and metering zone, while the clamping unit primarily contains and holds the mold (Figure 2.10). To begin the process, the thermoplastic pellets are fed into the first part of the plasticizing unit through the hopper, also called conveying zone, involving a reciprocating single screw injection. From here the material reaches the screw channel where the material experiences compaction and then is pushed further down the channel. In the next zone, i.e. transition zone, the material melts due to shear forces induced by the motion of the screw. This melted (or liquidified) material enters the metering zone where it homogenizes as a polymer melt containing fiber strands and is injected into the mold. This step of filling up the mold cavity with the melt is called filling. In the mold cavity, the melt is allowed to settle and allowed to solidify through cooling after filling. A back pressure is maintained to compensate for the material shrinkage due to cooling. This phase is called the packing phase. Soon, the material is given sufficient time to cool down and become stable as a final product, which is called the cooling phase. As the mold opens, the part is ejected, while the screw reciprocates and prepares for the next batch of the material to be fed. This process is

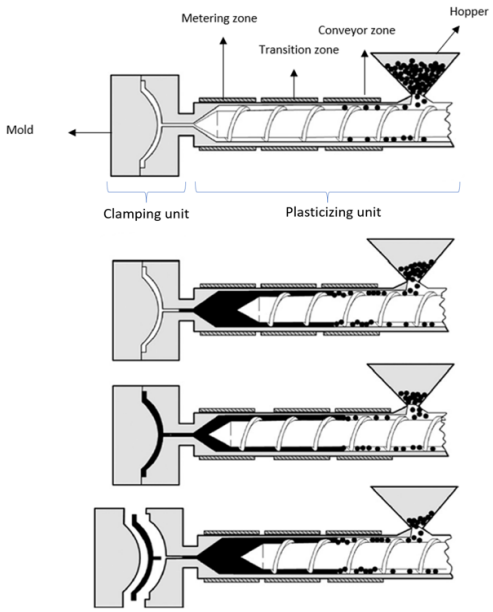

Figure 2.10: Schematic of injection molding process with different zones of processing. Adapted from [40].

repeated over again to produce large number of products ([8], [10], [40], [42]).

Therefore, in summary, the whole molding process is combination of the following steps [42]:

1. Mold closing
2. Injection/Filling
3. Packing
4. Cooling
5. Solidification and screw retraction
6. Ejection

FIBER LENGTH IN INJECTION MOLDING

In injection molded products, the length of a fiber in the composite product plays quite an important role in determining the mechanical properties of the composite [43]. This can also be observed from Figure 1.1, where increasing fiber lengths lead to better mechanical properties (in chapter 1). In the production process, fiber attrition is very commonly observed and has been tabulated in Table 2.3 based on the research. In the literature, fiber breakage reduction of about 80-95% has been observed in comparison to the initial fiber length [44].

Table 2.3: Some of the FRPs found in literature along with their breakage in during processing.(*Note: The fiber lengths (*) mentioned here are the number average fiber length)*

Material Description	Initial length (μm)	Final length in the melt (μm)	Reduction (%)	Reference
Long glass fiber reinforced PP	3200	425	87	[43]
Short glass fiber reinforced PP	350	160	55	[44]
Long glass fiber reinforced PP	7000	800	90	[44]
Long glass fiber reinforced PA*	7700	1500	81	[45]
Long glass fiber reinforced Nylon-6 (30 wt%)*	4500	141	97	[46]
Long glass fiber reinforced PP (20 wt%)	10000	1150	89	[47]
Long glass fiber reinforced PP (20 wt%)*	640	350	45	[48]

The decrease in fiber length by a significant amount is bound to result in deteriorated fiber mechanical properties. In order to utilize the full potential of the reinforcing effect of the fibers in the composite, a minimum amount of fiber length should be maintained in the final product ([49], [50]). This minimum fiber length is called the critical length and is given by the following equation [51]:

$$l_{crit} = \frac{\sigma_f r_f}{\tau_f} \tag{2.1}$$

Here, l_{crit} denotes the critical length above which the mechanical loads of the composite are shifted to the fibers from the matrix and full utilization of fibers is made. Further, σ_f is the tensile strength of the fiber, and r_f and τ_f are its radius and interfacial shear strength respectively. If the fiber breakage goes beyond this particular length, major load distribution shifts towards the matrix, and the composite reinforcement is lost. Therefore, it is highly important to understand and address the breakage in fiber length.

FIBER BREAKAGE IN INJECTION MOLDING

As discussed in the previous section, fiber breakage is rather common and quite extensive in the process of injection molding. Here, the breakage process is followed through the flow of the fibers through the injection plasticizing unit and the clamping unit. During the process, the melt passes through the following locations, where certain amount of attrition is observed [52].

1. The process begins when the polymers enter the screw extruder through the hopper for compounding. During this part, the screws severely damage the fibers through the action of rotation and extrusion. Maximum amount of fiber breakage is observed in this section.

2. After the material progresses into the next section of the injection molding unit, i.e. the conveying zone, the shear stresses and friction intensify on the fibers, further contributing to fiber attrition. In this section, as most fiber pellets are still solidified, fiber-fiber interaction also acts as a mechanism causing fiber breakage.

3. In the next zone, that is the transition zone, the material starts to melt and liquify due to the shear forces and friction caused by the screw and barrel walls. This contributes to fiber breakage; however, the degree of attrition decreases. The compression forces felt by the fibers, arising due to melt flow, also increase in this section.

4. In the metering section, most of the material liquefies and homogenizes. As a result, the fibers in this section are residual fibers which undergo minor fiber breakage.

5. Finally, the material is pushed into the mold where it experiences high pressure and forced to be shaped into a given geometry, which causes additional fiber breakage. Apart from the pressure, the geometry of the mold can also cause fiber breakage due to presence of tight spaces and corners.

Furthermore, the occasional placement of valves and gates, to control the motion of the melt can lead to fiber breakage as they may provide compressive stresses along with shear and friction on the fibers.
The breakage of the fiber, as explained in the steps above, is majorly attributed to the following three basic mechanisms.

(i) Fiber-melt interactions

(ii) Fiber-fiber interactions

(iii) Fiber-wall interactions

Fiber-melt interaction It involves the breakage of the fibers due to hydrodynamic stresses or shear stresses introduced on the fibers by the melt or matrix rheology. It is the most thoroughly addressed factor for fiber breakage in literatures studying fiber breakage in injection molding [53]–[55]. The general trend observed with increasing shear rates, and therefore increasing shear stress, is that the fiber attrition also increases.
The mechanisms suggested in the literature involve the breakage of the fiber due to bending or the buckling during the flow. This bending or buckling can happen on the fibers which get pushed through different layers of laminar flow or get stuck at one end in the solid fiber bundle, with other end protruding out, creating difference in drag forces experienced by the fibers ([56], [57]).

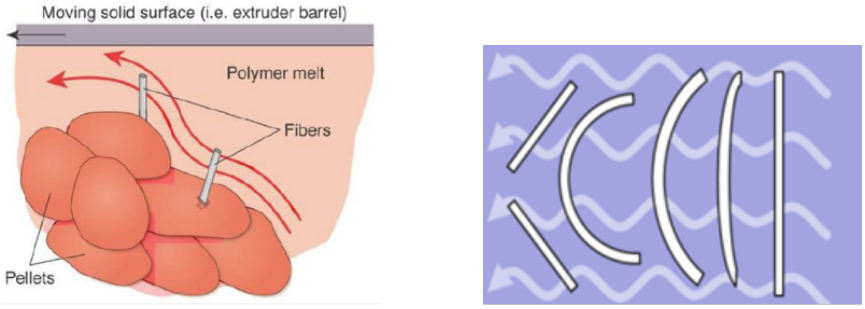

Figure 2.11: a. depiction of fiber breakage in the flow for the fibers anchored in the solid melt. Reproduced from [58] b. Fiber length breakage mechanism for the fibers completely submerged in the fluid flow of the polymer. Reproduced from [52].

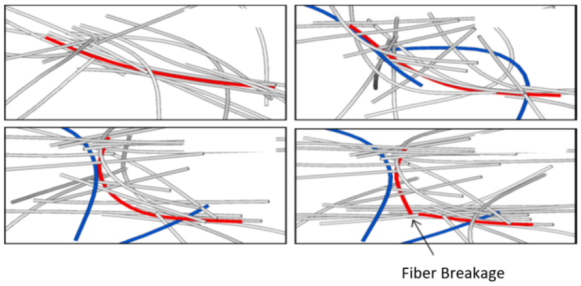

Figure 2.12: Fiber breakage mechanism for the fibers interacting with other fibers as depicted in the works of Sayasama et al. [60].

Fiber-fiber interaction As the name suggests, this method of fiber breakage refers to the interaction between the different fibers present in the flow of the melt leading or contributing towards the breakage of the fibers. The factor has been addressed in the literature through phenomenological as well as micro-mechanical models. The general trend observed suggests that the increasing concentration of the fibers lead to an increase in the fiber breakage, and has been addressed in the phenomenological models [59]. However, possible mechanism for this has also been suggested in literature, where a fiber can bend due to collective forces exerted by the other fibers in contact (refer to Figure 2.12) [60]. The fibers cause continuous bending of the particular fiber in question, and after certain time, its eventual breakage.

Fiber-wall interaction Apart from the fiber-fiber interaction and fiber-melt interaction, fiber interaction with the walls of the machine can also dictate fiber breakage. The mechanisms for fiber breakage are similar to that followed in fiber-fiber interaction, as the fiber protruding out of melt can face bending stress large enough to cause fiber failure. A schematic for possible mechanism is provided in the figure Figure 2.13.

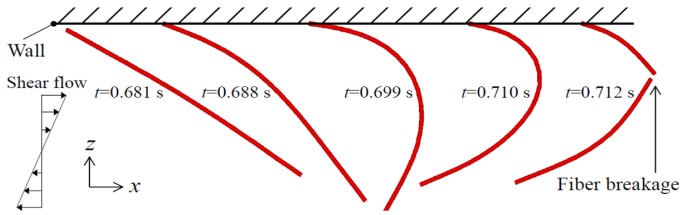

Figure 2.13: Fiber breakage mechanism activated for increasing time for the fibers at the walls or near the screw. Reproduced from [60].

As the figure represents, with increasing time, the bending of the fibers anchored at one end with the walls, increases, and eventually leads to breakage due to bending. Similar breakage mechanisms around the fiber walls are also presented in literature [52] in detail.

2.3. RESEARCH

2.3.1. EXPERIMENTAL RESEARCH

As mentioned above, fiber length is a highly important factor in determining the mechanical properties of the product during the process of injection molding. Therefore, it becomes equally important to address the breakage of fibers. Several studies have focused on the studying the breakage of fibers in different zones of injection molding process, to better understand and predict the breakage process itself. Turkovich and Erwin found most fiber attrition to happen in the melting (metering) zone, which is attributed to partially embedded fibers in the solid pellets which bend and shear during plastication ([43], [61]).

Patcharaphun and Opaskornkul [44] evaluated the fiber breakage property of glass fiber reinforced polypropylene in injection molding machine. They physically conducted fiber length measurements along the different sections of the screw to study the breakage in different zones.

The Figure 2.14 presents the observations where the percentage change in fiber length in each segment is presented with highest attrition occurring in the feed zone and compression zone for the material.

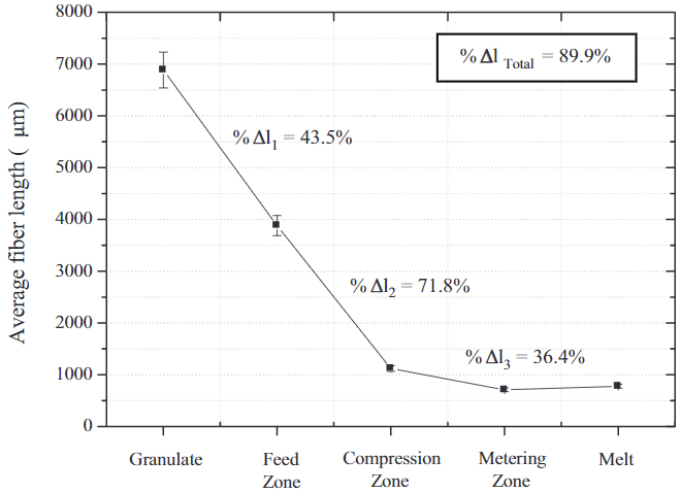

Figure 2.14: Fiber attrition trend observed in the helical section of solidified fibers melt obtained in [44].

These observations are further validated by Huang and Tseng [62] where a model is developed to verify these experimental results. They also tested different screw geometries and concluded that fiber breakage can be controlled by mitigating the compression forces generated during screw rotations. A recommendation to increase the channel depth at the feeding and the metering sections is made to decrease compression forces and prevent breakage.

Inoue et al. [63] have similarly tried to demonstrate the effect of screw geometry and

shape through experimental setups. In the designed experiment, they tested five different screws which are depicted in the Figure 2.15 and found that the screw design contributes to varying shear stresses along the fibers, and with reduced pitch, shear stress around the flow increases causing more fiber breakage.

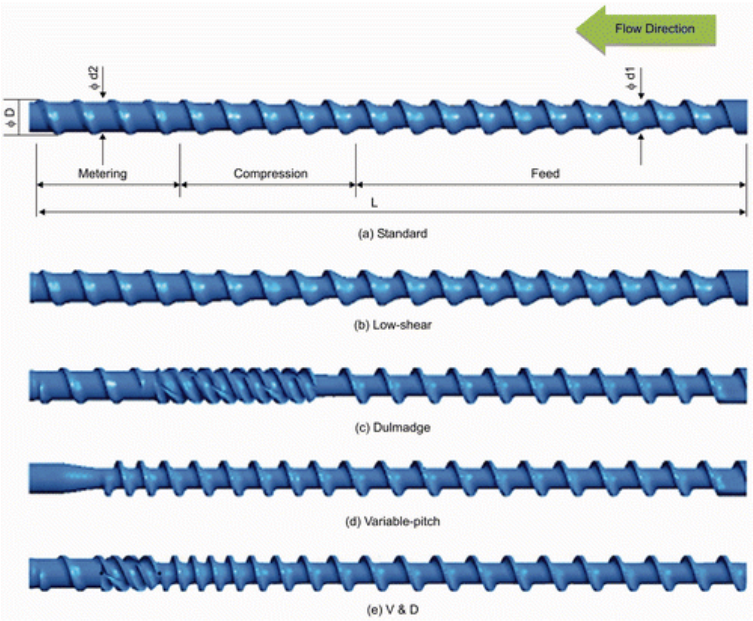

Figure 2.15: Different designs of the screws tested for study of fiber breakage in the work obtained from [63].

Other than the works involving the geometry studies of the injection extruder screw, some studies have conducted experiments to understand the influence of varying rotational speeds, shear rates and design of cavity molds.
Sometimes numerical data, such as shear rates, rotational velocities, viscosities and temperature, are quite difficult to extract from a injection screw. As a result, rotational rheometers such as couette or rotary rheometer are used. A couette rheometer allows for the 2-dimensional laminar flow of liquid between two cylindrical surfaces (as shown in Figure 2.16). The liquid material can contain solidified particles (representing fibers) between the two cylindrical surfaces and a known torque and revolutions can be applied to the inner cylinder to emulate the movement of injection mold. With customization, such as adding thermocouples, the temperatures, processing speeds and residence time of the flow melt can also be determined.

With the methodology of couette rheometer, various studies understanding the influence of processing conditions can be made. This method was adopted in the works of Inceoglu et al. [65] who determined that fiber breakage was dependent on screw speed, where laboratory based and industry-based extruder screws were tested for different screw speeds varying from 200-600 rpm.

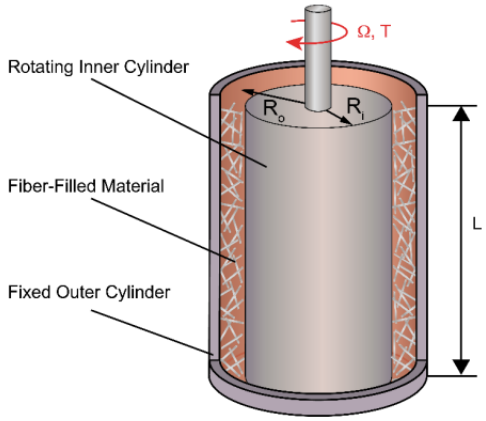

Figure 2.16: Basic depiction of a Couette Rheometer setup. Obtained from [64].

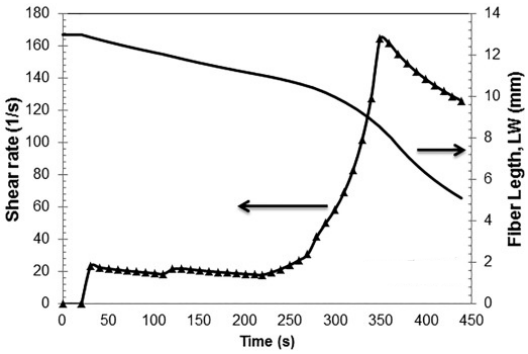

Figure 2.17: Experimental variation in the fiber length with increasing shear rate. Obtained from [62].

Huang and Tseng [62] present the fiber length variation with shear rate and present the results in Figure 2.17. The figure shows that the fiber length breakage increases with increasing shear rate.

Huang et al. [66] study the effect of the mold flow path on the fiber properties by conducting injection of fiber by designing two different melt fill paths, a right angular path or a square melt path and a round angular path with more smooth path.

Based on these designs, it was observed that in the square melt fill path, fibers could easily become entangled and their mechanical properties were poor with improper dispersion of fibers. On the other hand, round angle melt fill path showed less resistance to flow during the filling process and showed improvement in flow ability for longer melt flow lengths. This was also the case for the gates designed in the experiments, where flow ability and fiber properties were greatly improved by the large continuous filling sections provided by the rounded angle gate in comparison with the right-angle gate.

2.3.2. THEORETICAL RESEARCH

For the study of injection molding process, and to predict various flow conditions associated with it, various theoretical models have been developed. As mentioned in the subsection 2.2.4 already, injection molding process is charecterised primarily by the following steps [42]:

1. Mold closing
2. Injection/Filling
3. Packing
4. Cooling
5. Solidification and screw retraction
6. Ejection

Here, among the mentioned steps, most progress has been made in phases 2-4 [42]. While the remaining phases of the injection molding process are important in themselves, injection (or filling) phase has been significantly researched, as it involves highest fiber breakage rate. This section mainly covers the theoretical studies and developed mathematical models that address the fiber breakage phenomenon during the filling process.

One of the earliest works in the fiber breakage was conducted by Gupta et al. [56], who conducted a fiber breakage study for short and long fibers, using a screw extruder machine. The work concluded that major fiber attrition was the result of the fiber melt interaction at the melting zone in the extruder. The breakage mechanism suggested that the solid fibers protruding out into the melt flow of polymers experience drag forces, which cause fiber bending, and eventually breakage.

Forgacs and Mason [57], have also presented a similar breakage mechanism for fibers fully immersed in the melt flow where the fibers face axial bending due to varying velocity component along the fiber in the melt flow. These breakage mechanisms have been used as the foundation in many mechanistic models developed over the years to predict fiber breakage. They used Burgers' formulation [67] along with Euler's beam theory to derive an equation to estimate the critical product $\dot{\gamma}\eta$ at which a fiber would buckle under compressive stresses (here, $\dot{\gamma}$ is shear rate and η is viscosity) [59].

Shon et al. [68] developed a kinetic model for the evolution of the average fiber length, L, which decreases towards a residual, or unbreakable length, L_∞, using the following equation:

$$\frac{dL}{dt} = k_f (L - L_\infty) \tag{2.2}$$

Here, k_f is a breakage rate coefficient. The values for the parameters L_∞ and k_f were derived empirically from the set of experiments conducted in the study using a counter-rotating twin screw extruder.

In a similar work, Chen et al. [69] further tried to improvise on an existing exponential decay model with a kinetic decay constant and a critical length (Equation 2.3).

$$\frac{L(x) - L_{\text{crit}}}{L_0 - L_{\text{crit}}} = -e^{-K \times t} \tag{2.3}$$

Here, K is generalized breakage dynamic constant, L_0 is initial fiber and L_{crit} is the average fiber length. They adjusted certain parameters and performed a good fitting based

on the experimental results obtained from the molding of an end gated plaque produced with a lab scale single extruder.
Based on the models involving fitting, one of the most commonly used models is the Phelps model developed by Phelps et al. [53] and is also widely used in commercial softwares to predict fiber breakage. The model predicts the fiber length distribution based on the fiber buckling mechanism suggested in the works of Gupta et al. and Forgacs and Mason ([56], [57]). The buckling is based on the hydrodynamic forces faced by the fiber leading to its breakage. The model is phenomenological and predicts fiber length distribution based on a conservation equation which iteratively estimates the rate of fiber breakage based on the 'breakage probability' and 'child generation rate', where a 'child' fiber is a shorter fiber obtained from the breakage of a larger fiber. This has been explained in subsection 3.3.1.
Similar to the Phelps model, Durin et al. [54] also developed another continuum model for the prediction of the fiber breakage and fiber length distribution. The model, like Phelps, predicts fiber length distribution over time only assuming hydrodynamic force interaction among the fibers. Both the models are quite similar with major difference being the fact that Durin model assigns a non-zero breakage probability for fiber when the buckling load is less than the critical buckling load for the fiber, while critical buckling load in the Phelps model is defined as the load below which the fiber cannot break. For other differences between the models, the reader is referred to [53].
Inspired from the Durin's model, Kang et al. [55] in their work developed a mechanical model to predict the fiber breakage under the influence of shear stresses experienced from the flow of the melt filling. The breakage mechanism for the fibers was considered to be the buckling of the fibers based on the Euler buckling criterion. To verify the model with experimental results, they used glass fiber reinforced polypropylene (GF/PP) with extrusion simulations in a rotary rheometer to emulate the experiments with predetermined shear rates. The model in their work neglects the fiber-fiber interaction as a factor for fiber breakage, and therefore, experiments used fiber weight fraction of 10% to minimize the effect of fiber-to-fiber interaction on fiber length breakage.
The models discussed till now mostly involve just fiber melt interaction as a factor for calculating fiber breakage. However, Bechara et al. [59] further developed a design of experiments (DOE) employing a coutte rheometer to determine the correlations between processing conditions, material properties, fiber concentrations and fiber length reduction. The main purpose of the study was to develop a phenomenological model which could incorporate fiber-fiber interaction as a parameter for fiber length prediction during injection molding. In their work, they have used different concentration of GF/PP and have established a relation between different factors through a model.

These statistical models have been tested and validated for filling simulations in simple geometries such as ISO plaques and center-gated disks as they can be easily simplified into a 2D axisymmetric problem [59].

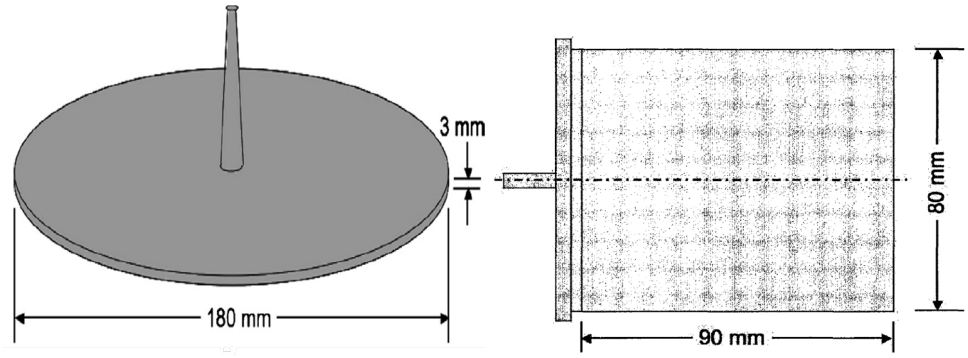

(a) (b)

Figure 2.18: Simplified geometries used in literature for the validation of filling simulation model (a) Center gated disk (b) ISO plaque. [70]

The above mentioned models are mostly statistical and estimate fiber breakage by fitting the models to experimental data. Few works have tried to just focus on improving this statistical prediction of fiber breakage in experiments, without working on the mechanics of the fiber breakage through modelling ([71], [72]). There are some other models which try to incorporate the other effects such as fiber-fiber and fiber-wall interaction.
Sayasama et al. [60] in their work have developed a model which uses direct particle simulation approach. The finite element approach considered in their work evaluates the shear stresses experienced by the individual fibers, which are considered as a chain of connected spheres. They find that the fiber length decreases with increasing viscosity, shear rate and fiber volume fraction. In their work, they also present a depiction of how fiber-fiber interaction and fiber-wall interaction can also lead to fiber breakage. Chang et al. [73] also developed a direct particle simulation based approach where the failure criterion for the breakage of a fiber was based on a critical radius. Each fiber was considered as a chain of rods that experience various hydrodynamic and interaction effects. Fiber failure was reported when the bending of fibers would surpass a critical radius.

2.4. RESEARCH CONCLUSIONS, GAPS AND OBJECTIVE

Based on the literature and theoretical background provided, there are several research questions that can be proposed. The research conclusion, gaps are provided in this section followed by the research objectives developed for this study.

2.4.1. RESEARCH CONCLUSIONS

The following research conclusions have been established:

1. Among the various production processes, injection molding is highly suitable for mass producing complex geometrical shapes with significant range of size.

2. Several experimental methods to evaluate the fiber breakage have been conducted,

specially along the plasticizing unit of the injection molding machine.

3. The major downside of the injection molding resides in the high costs of development of customised molds for the injection process. This makes study of fiber breakage more important to provide guidelines for the development of cavity geometries and save input costs.

4. The study of the fiber breakage using the experimental methods requires a lot of time. The process of extracting the mold and breaking it into smaller shapes followed by the extraction of thousands of smaller fiber for manual measurement is quite considerable. This has pushed the development of computational methods to measure and predict fiber breakage trends.

5. Several statistical and direct simulation methods have been developed aimed at predicting the fiber breakage. While statistical methods are based on experimental fitting and are much faster computationally, direct simulation methods tend to be more accurate and provide better overview of fiber breakage.

6. Statistical models have proven to predict well for basic geometries such as centred gated discs and ISO plaques and have been applied in commercial softwares for the prediction of fiber lengths.

2.4.2. RESEARCH GAPS AND OBJECTIVES

Based on the research conclusion presented above, research gaps are highlighted which have been used to establish the objectives of this work.They are enumerated as follows:

1. In the research conducted in this study, Phelps model has been the most widely applied commercial model. Studies have been conducted to understand fiber orientation and concentration in filling simulations, however, not enough work is focused on fiber length evaluation using simulation softwares.

2. There has been a lack of simulation studies that have been used to establish the relation between the rheological properties of the flow, such as shear rate and viscosities with fiber breakage in the cavities of injection mold.

3. The current state of the research involving the study of fiber breakage exists for very simple and basic geometries, such as centre gated discs or rectangular ISO plaque samples. Thus, there is a scope for understanding the breakage of fibers in slightly more involved geometry, which would present a much closer results to the practical shapes applied in industries.

4. The Phelps model [53] is the only statistical model widely applied in commercial softwares for injection molding. However, the model has not been yet properly tested for varying geometries and not enough guidelines are provided for tuning in such a situation.

5. The Bechara model [59] is another quite recent model aimed at predicting the fiber breakage in the filling simulation. However, the model has not been validated for a 3D dimensional filling simulation and compared with the Phelps model.

Thus, based on the above research gaps, following research objectives have been set-up for this work:

1. A study of influence of the geometry on the fiber breakage trends during filling of an injection molding process. This is done to understand how the rheology along with geometry influences fiber breakage, which in turn would help in providing better design guidelines for industrial use.

2. Evaluation of the currently applied commercial Phelps model for predicting fiber breakage, and understanding the amount of parametric tuning required for prediction, with changing geometries.

3. A comparative study of the Phelps model with a novel Bechara model, by creating an analytical model applied as a post-processor to the rheological properties obtained from simulation software. This is done to benchmark the models, scrutinize them, and propose better model of two, with a posibility of modification.

3

METHODOLOGY

This chapter covers all the important terminologies, models, and methodologies explained with detailed steps, that have been undertaken in this work to address the research objectives.

3.1. FIBER PROPERTIES

Other than the type of the fiber material itself, there are some other factors that decide the quality of the final composite product, making them relevant for the study. Fiber lengths, fiber orientation and fiber concentration are the primary factors determining the quality of the fiber, and are discussed further.

3.1.1. FIBER LENGTHS

For the composites, the mechanical, thermomechanical and electrical properties have been proven to be correlated with the fiber lengths. The properties of the composite seem to improve with increasing fiber length ([3], [4]). The fibers, based on their lengths have been classified into 3 major categories: short fibers, long fibers & continuous fibers. While short fibers usually range for a length of under 1 mm, long fibers length are estimated to be around 4-15 mm ([74], [75]). Continuous fibers are characterised by having a large fiber length-to-fiber diameter ratio, and therefore, are sometimes used interchangeably with long fibers as well [76].

3.1.2. FIBER ORIENTATION

Fiber orientation (FO), along with fiber lengths, also plays a notable role in the tensile strength and modulus properties of the composite matrix as discovered in the study [77]–[81]. While tensile strength and Young's modulus seem to decrease with more misalignment of the orientation ([78], [80], [81]), shear strength seems to decrease with increasing orientation angle [79]. Therefore, addressing fiber orientation during the production of the composite can also become an important step.

3.1.3. FIBER CONCENTRATION

The third important factor for addressing the properties of the composite is the concentration of the fiber. As fiber is reinforcing component of the composite for physical strength, increasing fiber concentration tends to improve mechanical strength of the composite, which has also been found in literature ([3], [81]). However, increasing the fiber concentration beyond a certain critical value can not lead to any further improvement, as the matrix concentration would be too low in the composite to provide support leading to voids and defects in the composite [81]. AS a result, an optimum concentration of fiber is usually preferred.

3.2. FIBER LENGTH MEASUREMENT

The estimation of accurate fiber lengths is a very important step in the process of understanding fiber attrition in injection molding. It helps in experimentally providing a tangible metric for evaluation of fiber lengths, which can be used to develop and validate new models and their underlying physics by providing accurate and reliable experimental data [53]. While there exists plenty of approaches for the measurement of fibers, no standard procedure has been accepted as the norm. Since even a small sample can contain millions of fiber pieces, the fiber measurement is slightly cumbersome.

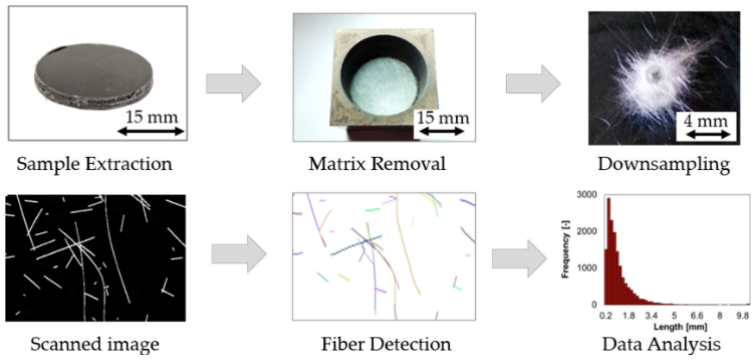

Figure 3.1: Fiber length measurement methodology as commonly observed in major approaches. Reproduced from [82].

Nonetheless, majority of approaches in fiber breakage share 4 basic steps [61]:

1. The part of the sample to be studied is extracted and then heated to a sufficient temperature. The process of heating the sample is called pyrolysis. This melts away the matrix of the sample, leaving behind only the fibers.
2. In the second step, the remaining samples of fibers are collected and prepared for a scanning procedure, also known as down sampling. In most approaches, the fibers are placed on a small glass plate containing a liquid solution, which helps with dispersing the fibers away.
3. In the next step, a digital image of the dispersed fibers is created using either an optical microscope, or optical document scanner (digital imaging).

4. Finally, a software is used to determine the lengths of the individual fibers by analysing the digital image of the fibers. The fibers are detected either manually in a software or with the help of automated or semi-automated image-processing algorithms.

The steps have also been represented in the Figure 3.1. While these are the common steps followed in the measurement of the fiber lengths, the details in the steps can vary to a certain degree in many of the approaches, and these differences have been addressed in the literature [61].

3.2.1. NUMBER AVERAGE AND WEIGHT AVERAGE FIBER LENGTHS

After the fiber length distributions (FLD) are obtained which indicate the fiber lengths and the corresponding number of fibers present (Figure 3.2), two measurements are introduced to quantify the distribution data essential for the theoretical study. These measurements are termed as the number average and weight average fiber lengths.

$$L_n = \frac{\sum N_i \ell_i}{\sum N_i} \tag{3.1}$$

$$L_w = \frac{\sum N_i \ell_i^2}{\sum N_i \ell_i} \tag{3.2}$$

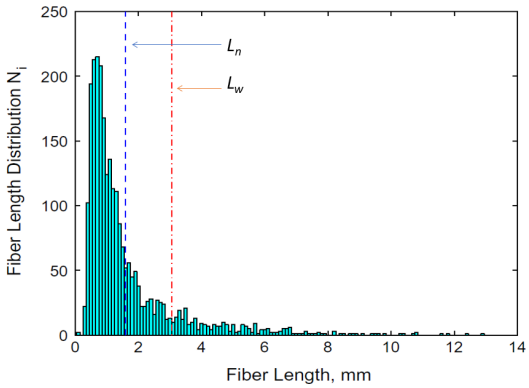

Figure 3.2: Fiber length distribution indicating the number average and the weight average fiber lengths. Adapted from [53].

Here, N denotes the number of a given fiber 'i' and l denotes the length of the fiber. The value of 'i' indicates the index of a fiber among all the fiber lengths that are present in the distribution. For example, if the smallest length is 0.5 mm and the largest length is 5 mm, with 10 bins containing all the lengths from 0.5 mm to 5 mm, then 'i' ranges from 1 to 10. These numbers are depicted in the Figure 3.2. In the figure, the blue line indicates number average, and the red line indicates the weight average fiber length.

3.3. SIMULATION MODELS

In this section, the model considered in this work for the study and prediction of fiber breakage have been explained and discussed.

3.3.1. PHELPS MODEL

It is a statistical model developed to predict the fiber length distribution for long fibers during the processing of fiber reinforced composites. The basic assumption of the model is that the fibers only break due to the hydrodynamic forces acting on it, which lead to fiber buckling, and ultimately, their breakage. Forces that may arise from other contacts, such as fiber-fiber interaction or fiber-wall interaction, are not considered.
The model is fundamentally based on the conservation of the total length of the fiber, and a basic constitutive equation is used to ensure this conservation. This is denoted by Equation 3.3:

$$\frac{dN_i}{dt} = -P_i N_i + \sum_k R_{ik} N_k \tag{3.3}$$

Here, N_i represents the number of fibers of a specific length ℓ_i (where 'i' is the index of the given fiber), and therefore, the equations represents the rate of change of number of fibers. Further, $P_i N_i$ represents breakage rate, or the loss of fibers of ℓ_i length due to breakage, $R_{ik} N_k$ represents the generations of fibers of ℓ_i length due to breakage of longer fibers (ℓ_k). The subscripts i and k represent the discretization of the fiber lengths possible. For instance if a fiber of l_{max} = 6 mm is considered, with a smallest resolution of the length to be Δl = 100 μm for computation, then i can vary from 1 to a maximum of M, where $M = l_{max}/\Delta l$ will denote the total number of discretizations possible.
To define the breakage rate, a constitutive equation is defined based on the assumed forces acting on the fibers. As mentioned already, the deformation for fiber breakage assumed in this model is fiber buckling, which provides a equation of buckling ratio obtained from equating to the hydrodynamic stresses to the buckling strength of the fiber. This critical buckling ratio is given by (Equation 3.4):

$$B_i \equiv \frac{4\zeta \eta_m \dot{\gamma} \ell_i^4}{\pi^3 E_f d_f^4} \tag{3.4}$$

Here, B_i is critical buckling ratio, ζ is called the hydrodynamic drag coefficient, η_m is the viscosity of the polymer matrix, $\dot{\gamma}$ is the shear rate, E_f is the elastic modulus and d_f is the fiber diameter, and ℓ_i is the length of the fiber. This equation is derived from the Euler buckling theory. Based on the Eular buckling, a minimum fiber length is defined, below which, the fiber can not break. This is given by the following equation:

$$L_{ub} \equiv \left(\frac{\pi^3 E_f d_f^4}{4\zeta \eta_m \dot{\gamma}} \right)^{1/4} \tag{3.5}$$

If the buckling ratio (B_i) is less than 1, then the model assumes that the fiber breakage does not take place. The breakage is only assumed if the critical buckling ratio is

achieved. With the buckling ratio defined, breakage rate or probability is determined, with the variable C_B, known as the breakage coefficient, used as another factor:

$$P_i = \begin{cases} 0 & \text{for} \quad B_i < 1 \\ C_B \dot{\gamma} \left[1 - \exp\left(1 - B_i\right)\right] & \text{for} \quad B_i \geqslant 1 \end{cases} \tag{3.6}$$

Other than breakage probability, the other term involved in Equation 3.3 contains the 'child generation rate', which is the rate at which the longer fibers break to generate fiber of the given length. For this, the model assumes that breakage probability for any fiber is maximum at its centre. Therefore, for the fiber of length ℓ_i to be a generated from a parent fiber of length ℓ_k, the models predicts a normal probability distribution function (a gaussian profile), which is given by:

$$R_{ik} = \alpha_k N_{\text{PDF}} \left(\ell_i, \frac{\ell_k}{2}, S\ell_k\right) \tag{3.7}$$

Here, α_k is a scale factor chosen to normalize R_{ik}, ℓ_i is the fiber length with $\frac{\ell_k}{2}$ as the mean length, $S\ell_k$ as the standard deviation.

With the given equations, the Phelps model can be used to develop the fiber length distributions for a given fiber material of defined diameters and length, with selection of suitable fitting parameters, namely, breakage coefficient (C_B), drag coefficient (ζ) and scalar factor (S).

3.3.2. BECHARA MODEL

Similar to Phelps Model, Bechara model is another phenomenological model which aims to predict fiber breakage in an injection molded cavity for long fiber reinforced thermoplastics. The model involves the tracking of averaged fiber lengths (L_n & L_w) with time. The model proposes that the fiber length reduction over time follows an exponential decay with time towards an equilibrium value (as suggested by Shon et al. ([68]), which can be demostrated by the following equations (Equation 3.8 & Equation 3.9):

$$\frac{dL_N}{dt} = -k_{N,f}\left(L_N - L_{N,\infty}\right) \tag{3.8}$$

$$\frac{dL_W}{dt} = -k_{W,f}\left(L_W - L_{W,\infty}\right) \tag{3.9}$$

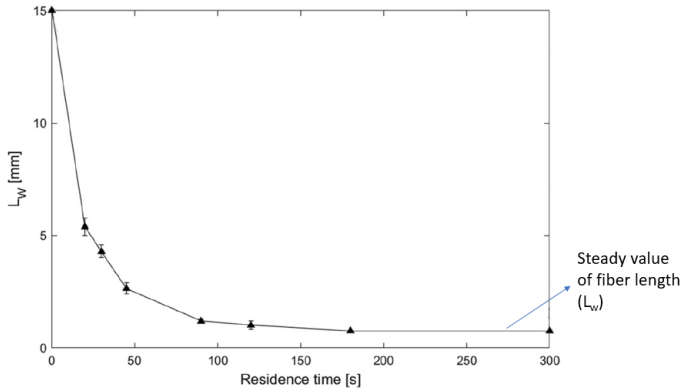

Figure 3.3: Weight averaged fiber length (L_w) decay over time to a steady length. Adapted from [59].

These equations provide the constitutive framework on which the fiber breakage over time is evaluated. Here, L denotes the averaged length of the fiber, whereas k_f and L_∞ are the parameters for the state equation, and represent the breakage rate and the equilibrium length, respectively.

With the state equation defined, the model presents relevant equations for the parameters for their calculation. L_∞ in this model, is similar to the unbreakable length (L_{ub}), as defined in the Phelps model (subsection 3.3.1). The expression for L_∞ is derived by assuming a bending deformation, under the presence of various, hydrodynamic and interaction forces between fibers and walls. With bending deformation assumed, the expression for L_∞ becomes:

$$L_\infty = \lambda \left(\frac{\sigma_u d_f^2}{\eta_m \dot{\gamma}} \right)^{1/2} \tag{3.10}$$

Here, σ_u is the ultimate strength of the fiber, d_f is the fiber diameter, η_m is the viscosity and $\dot{\gamma}$ is the shear rate of the flow. The coefficient λ is introduced as a fitting parameter in the model, to account for the effect of the fiber-fiber and fiber-wall interactions leading to fiber breakage.

The parameter k_f denotes the breakage rate of fiber, indicating how often the fibers break. The expression for the same is given as:

$$k_f = \xi \dot{\gamma} \tag{3.11}$$

The Equation 3.11 indicates that the breakage rate is directly dependent on shear rate of the fluid environment. This direct dependence is calculated using the coefficient ξ, which is the fitting parameter for the rate of deformation/breakage. Thus, with the given equations, the Bechara model can be replicated based on the two fitting parameters, namely breakage rate coefficient (ξ) and the fiber interaction coefficient (λ).

3.4. SIMULATION STUDY

A simulation study was performed on certain geometrical samples to predict and measure the experimental data available at hand using a software. The simulation study is performed using the injection molding software Moldex3D, which involves a module to calculate the fiber breakage in a injection molded cavity and estimate residual fiber lengths at different stages of filling.

The software allows the simulation of injection molding process itself by incorporating various stages of injection, such as filling, packing and cooling phases, through a set of equations, and associated boundary conditions, that create a mathematical model of the molding simulation. Apart from defining the physics of the mold filling simulation through the equations, the software also requires an estimation of properties of the material and the geometrical complexity of the model. All of these computational modules are integrated into the Moldex3D software already. However, in this work, the focus is placed on the fiber breakage model included in the software and its use to predict the experimental observations.

To progress with performing the simulation study, a set of geometries have been developed and used for mold filling experiments in the injection molding unit at Brightlands Materials Center (TNO Facility) situated at Geleen.

The geometries are presented in Figure 3.4 and present different possible orifice thicknesses. The idea behind these geometries is to address the fiber breakage in slightly more complicated designs than the ones observed in literature and to understand how rheology properties and different thicknesses or cross-sectional areas of the geometries can influence fiber breakage. This is also done by keeping in mind the first research objective proposed in this work, and to propose relevant design guidelines to the designers in the industry.

An experimental injection molding process for each of the geometry has been performed and the fiber lengths have been measured for the samples at different sections

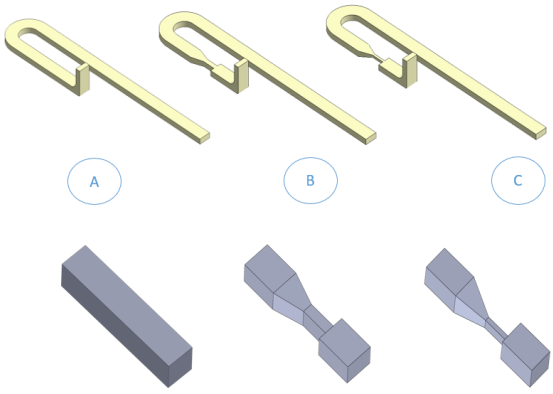

Figure 3.4: Sample geometries considered in this study to understand the influence of geometric variation of fiber breakage.

using the method mentioned in section 3.2. The fibers have been measured along the sections as represented in Figure 3.5 and the properties of the fiber (glass fiber 30%) used in the complete study have been mention in Table 3.2.

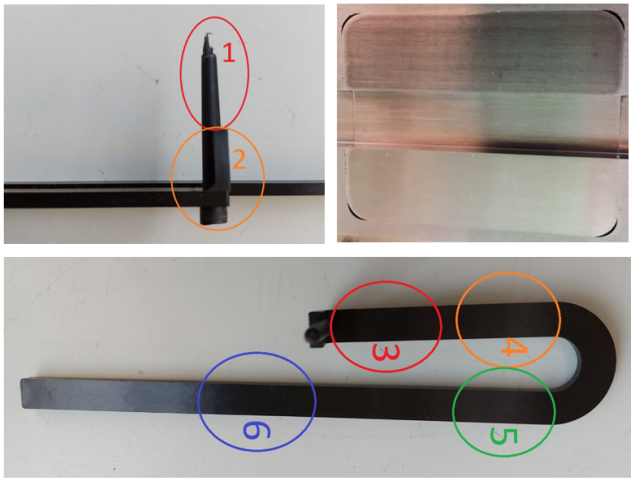

(a)

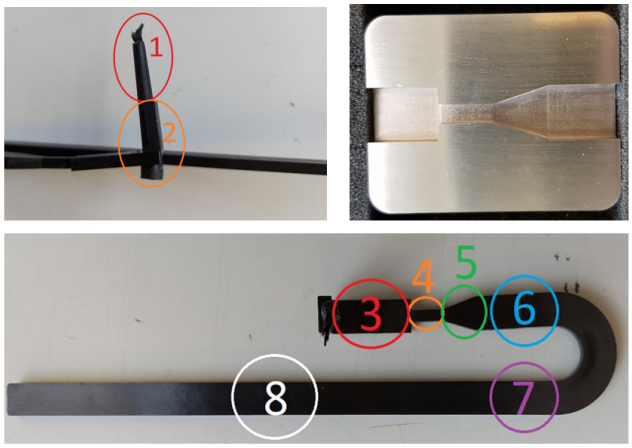

(b)

Figure 3.5: Sections defined for each of the geometries for the measurement of the fiber length distribution and averaged fiber lengths for experimental data for (a) Insert A (b) Insert B

As shown in Figure 3.5, the fiber distribution, and in turn, fiber lengths, for each of the section are separately measured and evaluated. After the measurements were performed for different geometries, the results were obtained for the fiber lengths observed along the different sections. These lengths are presented in the Figure 3.6 and the Table 3.1.

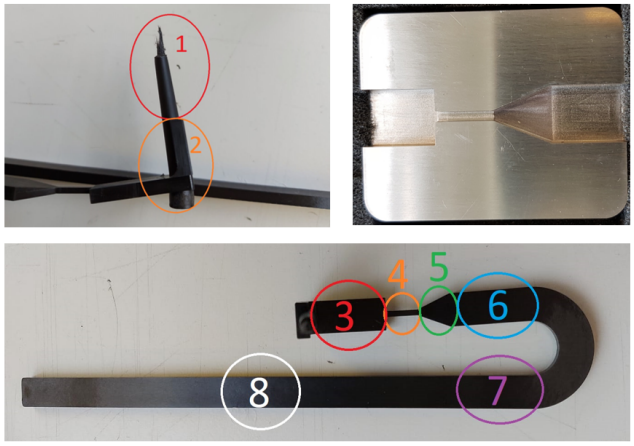

(c)

Figure 3.5: **(CONTD.)** Sections defined for each of the geometries for the measurement of the fiber length distribution and averaged fiber lengths for experimental data for (c) Insert C.

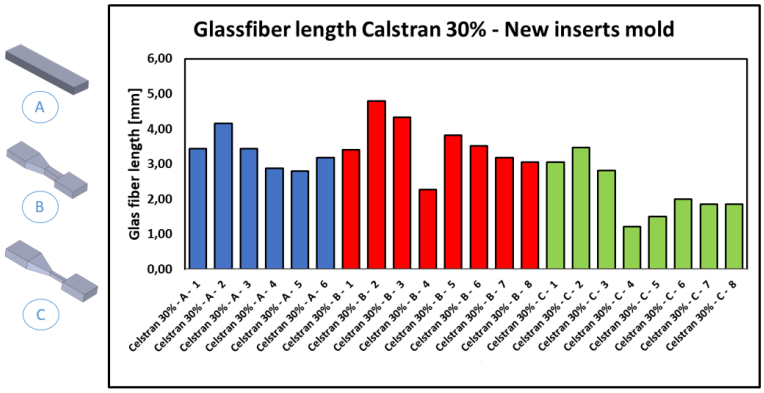

Figure 3.6: Weight averaged fiber lengths (L_w) as obtained for each of the inserts for the corresponding sections/position.

To perform the geometric simulation study of the experimental results obtained above, the next step becomes to transfer the study to a simulation environment of Moldex3D software. This is done by first creating a model of the geometry (a STEP file) using a CAD software, such as SolidWorks, in this case.

Table 3.1: Weight averaged fiber lengths L_w as observed from the experiments for different insert geometries.

Mold insert	Position	Material with insert and position	Amount of fibers	weigth averaged fiber length Lw	Standard Deviation
A	1	Celstran 30% - A - 1	27093	3.43	0.018
A	2	Celstran 30% - A - 2	22254	4.16	0.021
A	3	Celstran 30% - A - 3	21190	3.43	0.022
A	4	Celstran 30% - A - 4	29174	2.88	0.017
A	5	Celstran 30% - A - 5	17064	2.80	0.017
A	6	Celstran 30% - A - 6	17602	3.18	0.021
B	1	Celstran 30% - B - 1	17415	3.40	0.020
B	2	Celstran 30% - B - 2	11002	4.79	0.021
B	3	Celstran 30% - B - 3	12307	4.33	0.021
B	4	Celstran 30% - B - 4	16867	2.27	0.025
B	5	Celstran 30% - B - 5	13591	3.82	0.023
B	6	Celstran 30% - B - 6	14065	3.51	0.021
B	7	Celstran 30% - B - 7	23153	3.18	0.019
B	8	Celstran 30% - B - 8	26402	3.06	0.017
C	1	Celstran 30% - C - 1	32462	3.05	0.020
C	2	Celstran 30% - C - 2	23061	3.47	0.020
C	3	Celstran 30% - C - 3	28340	2.82	0.016
C	4	Celstran 30% - C - 4	14877	1.22	0.011
C	5	Celstran 30% - C - 5	37513	1.51	0.010
C	6	Celstran 30% - C - 6	45051	2.00	0.012
C	7	Celstran 30% - C - 7	44034	1.86	0.010
C	8	Celstran 30% - C - 8	44636	1.85	0.010

The steps necessary for the creation of the final mesh in the Moldex3D software after the development of the STEP files are as follows:

1. The STEP file for the geometry was imported into the Moldex3D designer environment,
2. An inlet face was defined on the geometry using the 'Melt Inlet' tool (Figure 3.7). The inlet face in the simulation provides the entrance of the polymer melt into the cavity mold.

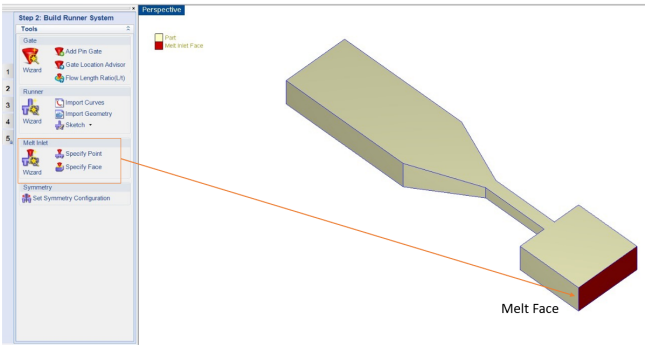

Figure 3.7: Melt inlet face defined for the insert C in the Moldex3D designer environment.

3. To evaluate the filling simulation results, it becomes important to assign certain nodal points to extract the information relevant to fiber breakage from. This was

done by adding the nodes manually at the required locations through the Moldex3D software. These node are called the 'measure nodes' in the software (Figure 3.8).

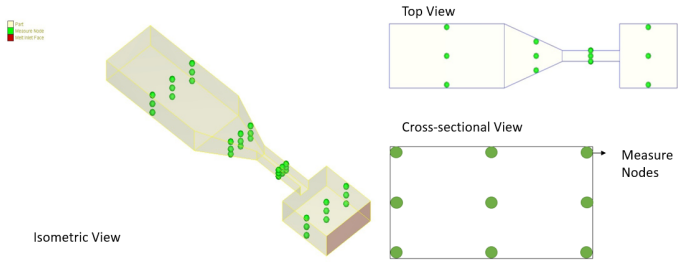

Figure 3.8: Measure nodes assigned to the insert C model for the measurement of the fiber lengths as obtained from the simulations.

To ensure that these nodes are corresponding to the experimental measurements, they are assigned at the locations where fiber lengths were measured in the experimental samples. This can be seen in the Figure 3.5.

4. The next step is to finally define the mesh on the geometry. Mesh fineness is determined by the trade-off between the accuracy of the results needed and the computational time allowed. This is usually determined by conducting a mesh convergence study which is explained in the Appendix C.

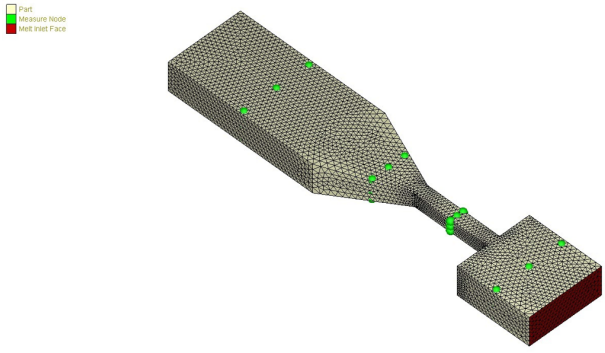

Figure 3.9: Meshed model of the insert C developed with defined measure nodes.

The developed sample mesh is presented in the Figure 3.9. After the necessary steps were performed for the creation of the mesh files, the next objective was to develop the simulation runs in the Moldex3D studio software, and perform the analyses. A number of steps were followed during the creation of a single run in the software. These steps are mentioned as follows:

1. To begin with, the developed mesh geometry was imported into the software.

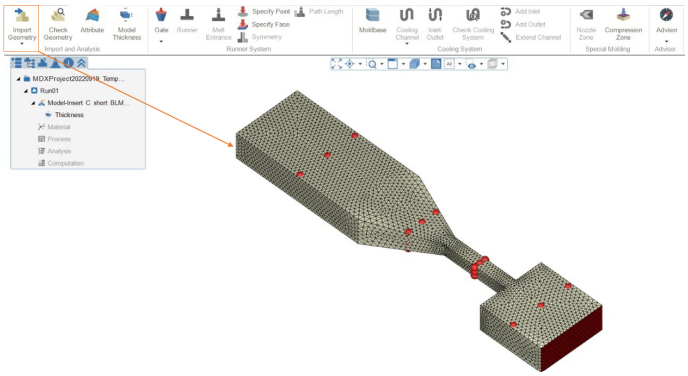

Figure 3.10: Importing the developed insert meshed geometry into the studio environment.

2. The next task was to define the material for the filling simulation. Moldex3D materials data bank provides a large range of materials with different polymer resins and reinforced fiber materials (Figure 3.11). Materials have been modelled with various properties already, such as PVT relations, viscoelastic behaviour and mechanical properties, to name a few, The user can chose the material based on the study that they want to conduct. The work is performed in this study on Glass fiber 30% reinforced polypropylene (GF30PP), which is the material on which the physical experiments have been conducted. The material properties of the fiber used in this study are presented in Table 3.2.

Table 3.2: Fiber properties of 30% glass fiber used in the study.

Property	**Value**
Density (g/cm^3)	2.56
Ultimate tensile (MPa)	2600
Young's Modulus (Gpa)	73
Diameter (μm)	12

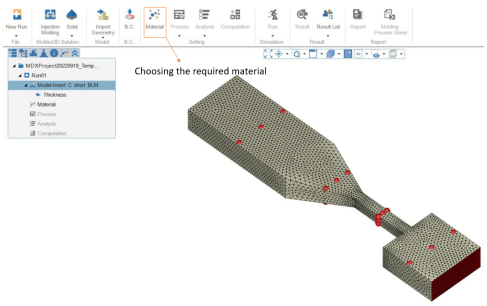

(a)

(b)

Figure 3.11: Assignment of the material property for the insert C meshed model using the software material data bank.

3. After defining the material, processing conditions were defined in the software representative of actual processing conditions. This enables the software to perform the mathematical simulation of the actual experiments with the real-life input data, and provide as realistic results as possible. Various filling simulations results, such as melt front time, temperature and pressure distribution, flow rheologies etc. tend to be influenced by these inputs.

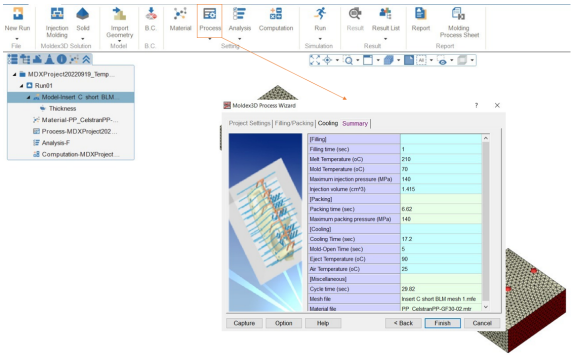

Figure 3.12: Selection of the processing conditions for the insert for the simulation.

4. To perform the fiber breakage analysis in the software, computation parameter needs to be modified in the software. The computation parameter defines the computational time steps to record the filling results. Further, to activate the fiber breakage analysis, the fiber breakage calculation needs to be activated as a post-processor in advanced filler parameter setting of computation parameter dialogue box. For input, the user can define the fiber diameter and aspect ratio, along with Phelps model parameters (which has been defined in subsection 3.3.1).

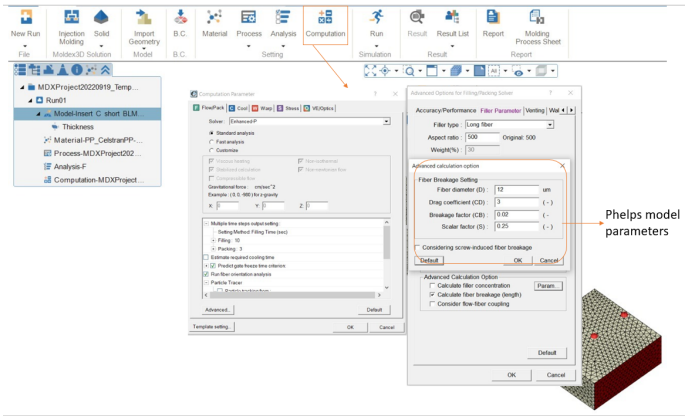

Figure 3.13: Assignment of the computational parameters involving the selection of the Phelps model parameters.

Since, the user can control a total of 3 parameters associated with the Phelps model for predicting the fiber breakage, the software predicted fiber breakage can be represented as a function of these 3 parameters, with the following equation:

$$FB = f(S, C_B, \zeta) \tag{3.12}$$

Here, S is the scalar factor, C_B is the fiber breakage coefficient and ζ is drag coefficient, all part of Phelps model. The user can tune the fiber length distribution along the geometry by fine tuning these 3 factors and produce agreeable results.

5. Finally, after defining the parameter and processing conditions as input, the simulation can be run with filling analysis option to perform the computational mold filling of the given geometry.

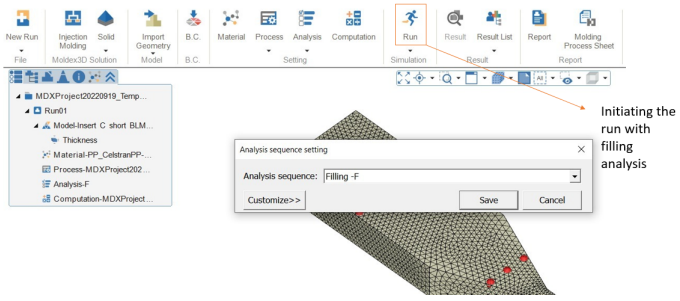

Figure 3.14: Setting the filling analysis sequence to define the final condition before starting the run.

Therefore, with the aforementioned methodology, the simulation study has been performed in injection molding software.

3.5. ANALYTICAL STUDY

The analytical study comprises of developing the numerical models for the fiber breakage study, and using them as post-processors to the flow data obtained from the injection molding simulation in Moldex3D. The analytical development of the breakage models is important because of the following reasons:

1. To perform the post-processing of the simulations manually and save computational times associated with creating full simulations. With the models integrated into the softwares, separate post-processing of the data is not possible and complete injection filling simulations need to be created. This leads to significant computational times.
2. To evaluate and compare models. Flow data obtained from the simulations can be used as input to the analytical models developed, and comparative studies can be conducted. This also allows for a greater degree of freedom to tune the model parameters and conduct a thorough study.
3. To modify or propose improvements to the models. Based on the results obtained from the analytical models, their shortcomings can be addressed. This could help in making suitable suggestion or provide radical modifications to the model.
4. To gain better control over the nodal fiber length distribution. In the software, the fiber lengths are automatically calculated with single input of fiber length from the user. However, to better understand the influence of rheology and varying fiber inputs on fiber breakage, better control of the nodal data is needed.

To perform the analytical study manually, two important steps are required:

1. Extracting and pre-processing the relevant nodal information from the simulation run.
2. Creating the mathematical model through a code to predict fiber length distribution as a post-processor using the nodal information provided as input.

Through the first step, all the important flow rheology properties of filling results obtained during the simulation need to be extracted. These properties could be the flow velocity vectors, viscosity and shear rate at different times and locations of the geometry, to name a few.

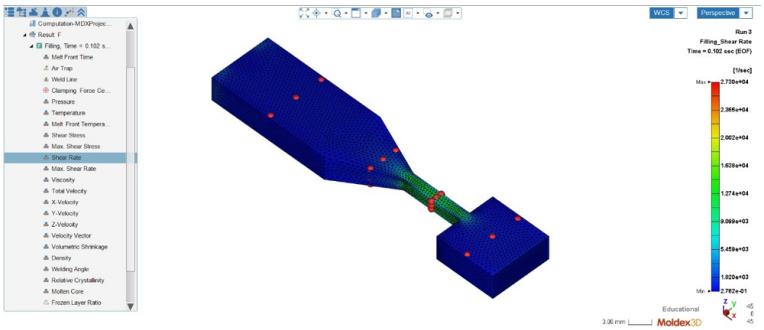

Figure 3.15: Filling results obtained from the simulation run, which can be used as the inputs to the analytical models for fiber breakage calculations.

This was performed using a python script where the user can input the coordinates of the nodal points and the corresponding information that the user intends to extract. Once, the nodal information is extracted, it was stored in a CSV file, which was later used as an input for performing the second step of analytical study.

The second step of the analytical study is more critical step, as it involves the post-processing of the data itself in fiber breakage prediction model. In this work, the analytical study is performed for the Phelps model and the Bechara model, and their analytical model are explained ahead.

3.5.1. PHELPS MODEL: ANALYTICAL

The Phelps model is the first model implemented using a MATLAB script as a post-processor to the simulations data. The Phelps model is chosen as it is the only model commercially applied for the prediction of fiber breakage in injection molding simulations softwares (such as Moldex3D itself).

To implement the Phelps model in the MATLAB code, the discretization of the constitutive equation of the model (subsection 3.3.1) has been performed as explained in [70].

To begin with the discretization, the constitutive Equation 3.3 for conservation of total fiber length is represented as follows:

$$N_{i,j+1} = N_{i,j} - P_i N_{i,j} \Delta t + \sum_{k|k\geq i}^{M} R_{ik} N_{k,j} \Delta t \tag{3.13}$$

Here, j is the discretization of time, where as i and k are the discretization of the fiber lengths, where k denotes the 'child' fiber generated from the 'parent' fiber i. M denotes, the maximum number of discretization possible with $M = l_{max}/\Delta l$ (already mention in subsection 3.3.1). Therefore, this will change the child generation rate (Equation 3.7) to following:

$$R_{ik} = \alpha_k N_{\text{PDF}} \left(i\Delta l, \frac{k\Delta l}{2}, Sk\Delta l \right) \tag{3.14}$$

$$\sum_j R_{ji} = 2P_i \tag{3.15}$$

The fiber breakage rate equation (Equation 3.6) follows the same discretization as before.

With the discretization performed, the fiber length distribution for a single point can be calculated with time. To perform the simulations with Equation 3.13, the test case performed in section 5.4 of [70] can be reproduced to check the code. This test case was replicated successfully, and the results are presented in Appendix A.

Therefore, with the verification of the model for a single point, the analytical model was applied as a post-processor for a 3 dimensional geometry to the simulation data obtained from step 1. This is in congruence with the method described by the [53].

3.5.2. BECHARA MODEL: ANALYTICAL

Bechara model is the second model used for discretization in this study. It is also a phenomenological model like Phelps, and estimates the fiber breakage through the evaluation of averaged fiber lengths over time in the cavity during the mold filling process.

The model has been discretized in a manner similar to Phelps model, and therefore, Equation 3.8 and Equation 3.9 have been modified to the following equations:

$$L_{N,j+1} = L_{N,j} - k_{N,f}\left(L_N - L_{N,\infty}\right) \tag{3.16}$$

$$L_{W,j+1} = L_{W,j} - k_{W,f}\left(L_W - L_{W,\infty}\right) \tag{3.17}$$

Here, j is the discretization of time, whereas all the other terms hold the same denotation as in Equation 3.8 and Equation 3.9. With this discretization defined, the model can be directly input as a post-processor to the simulation data, with parameter equations, Equation 3.10 and Equation 3.11 applied directly using the model parameters as input.

3.5.3. MODELLING APPLICATION METHOD

In this section, the methodology for the application of the models is explained in the geometry. The geometry of the model is assumed to be defined by the measure nodes where information is extracted from, in the software. The example is given in the Figure 3.16.

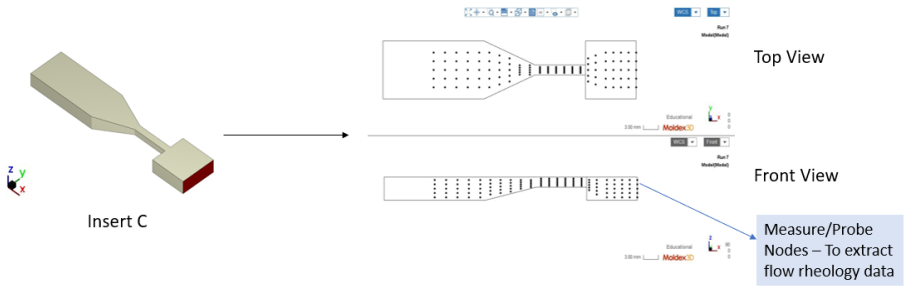

Figure 3.16: Discretisation of the geometry into nodes for the extraction of the flow results as inputs to the analytical model.

The probes are assigned to the locations in a manner such that the nodes are representative of the actual geometry used. They are connected in a layered structure such that the flow is captured properly to understand the influence of shear rates and flow viscosity. This can be seen in the Figure 3.17.

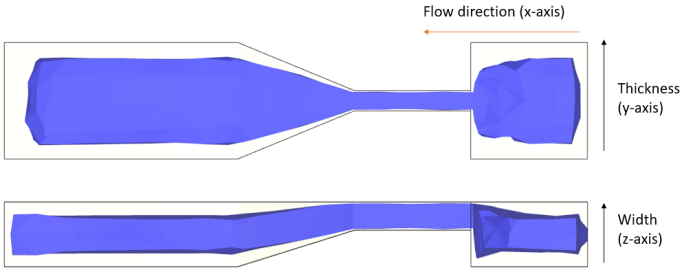

Figure 3.17: Flow velocity profile as observed in the simulation used for assignment of nodes to represent the geometry.

The probes are then filled in the order in which the flow information (shear rates and viscosity) is obtained from the simulation software. Thus, for every probe, the fiber breakage model is applied based on the rheology properties at the given location and time step, and then the observed fiber length or distribution is passed on to the next probe in the given layer for the next time step, ensuring a flowing medium. The layers are repeated in the thickness as well as in the width direction, to obtain the final 3D structure of the model.

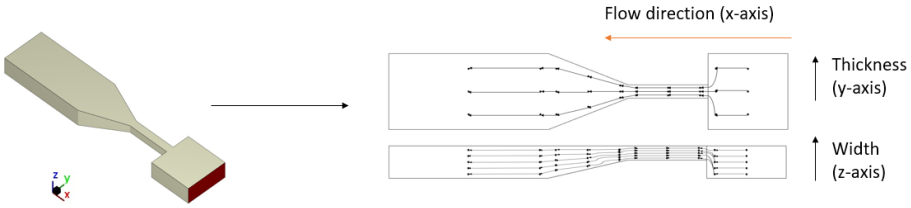

Figure 3.18: Layered discretisation of the sampled geometry to obtain a proper connection between the nodes to establish proper material transfer between the nodes during filling.

3.6. MODEL COMPARISON

In this section, a general comparison is made between the two models chosen in this study, Phelps model and Bechara model. The arguments for chosing the models are presented along with the similarities and the differences of the models.

The Phelps model is chosen as it is one of the most widely applied model in the simulation softwares for injection molding process, and is also integrated into the moldex3D software, which is the part of this study. It has been applied in the literature in numerous studies for relatively simpler geometries. This presents for a nice opportunity to study the application of the model for a more involved geometry. Apart from the popularity of the model, it is also quite computational time friendly, as it develops a phenomenological approach for the calculation of fiber breakage, rather than applying a direct simulation approach, where fiber breakage is calculated by including all the relevant forces needed at individual fiber level.

The Bechara model is chosen as it is a pretty novel model for the calculation of fiber breakage, and tries to tackle the breakage assumptions of the Phelps models, by incorporating the fiber-fiber and fiber-wall interactions into breakage mechanisms. It is also a phenomenological model, therefore, making it computational time friendly as well. Being a relatively new model, it offers a scope of modification and further improvement as well.

While comparing the two models directly, there are certain similarities that can be noted. As already mentioned, both of the models are phenomenological models, implying that they are developed by fitting the model parameters to the experimental observations for tuning. While Phelps model involves three fitting parameters, namely the scalar factor (S), the fiber breakage coefficient (C_B) and drag coefficient (ζ), the Bechara model includes breakage rate parameter (ξ) and the fiber interaction parameter (λ). Both, the models further are developed around an unbreakable length term, which are expressed as Equation 3.5 for Phelps model and Equation 3.10 for Bechara model. However, the derivation of these lengths belong to different breakage mechanisms, where L_{ub} is obtained from Euler buckling failure, while L_∞ is obtained by assuming a bending failure mechanism.

The major difference between the two models is that Phelps model estimates fiber breakage over time using the fiber length distribution at individual nodes and time steps (Equation 3.3), while the Bechara model does so by calculating the evolution of weight averaged and number averaged fiber lengths (Equation 3.9 & Equation 3.8).

4

RESULTS

With the methodology explained in the chapter 3, the results have been obtained for both, the simulation study as well as analytical study. The steps followed to obtain the results as well as the results themselves are explained in much detail for each of the study.

4.1. SIMULATION RESULTS

To begin with the simulations, a choice was made to select a particular geometry to perform the experimental prediction and parameter fitting. Among the geometries available for the selection (Figure 3.4), insert C was chosen as the model geometry. This decision was based on the fact that insert C involved most geometric variations in terms of cross-section area and should encompass the complexity of a more practical geometry. Therefore, the model was developed until the section 6 (as described in Figure 3.5) in the CAD environment, SolidWorks.

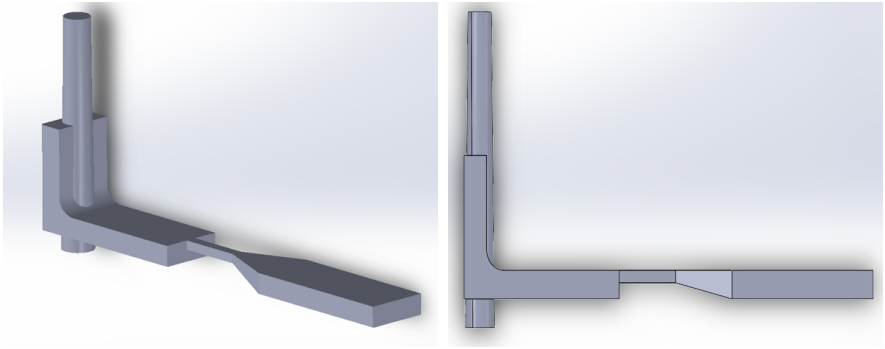

Figure 4.1: Insert C geometry model developed in the solidworks.

The model was then imported into the Moldex3D Designer software and then steps

Table 4.1: Processing parameters used for simulation studies in moldex3D.

Molding Parameter	Value
Melt temperature (°C)	270
Mold temperature (°C)	80
Max injection pressure (MPa)	140
Filling time (s)	1

Table 4.2: Input computational parameters for the initial study in the Moldex3D software.

Scalar factor (S)	Breakage coefficient (C_B)	Drag coefficient (ζ)	Aspect ratio
1	0.03	0.55	250

mentioned in section 3.4 were performed to create a final mesh for developing simulation runs.

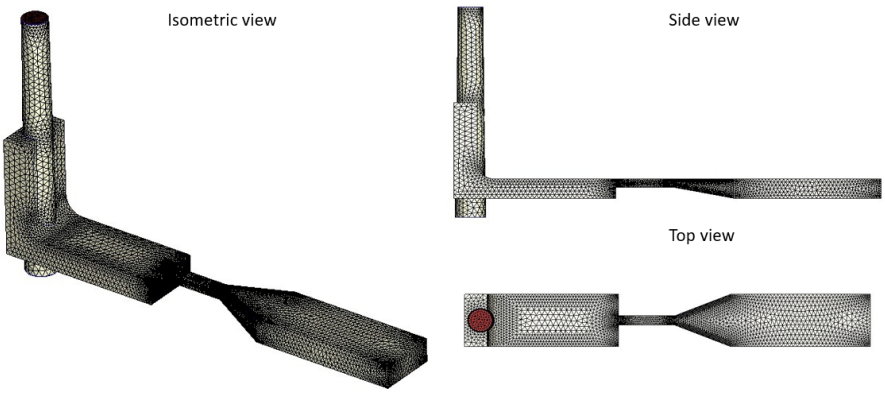

Figure 4.2: Final meshed insert C developed for the simulation study in the moldex3D

With the geometric model fully developed and the measured nodes created at the required locations, a baseline run was created. For processing conditions to run the simulations are shown in Table 4.1. The material selected is Celstran-PP-GF30 from the material database. For the parameters of Phelps model for computational, a reference value for each of the parameters was taken from the literature. Scalar factor (S) of 1.0, breakage factor (C_B) of 0.03 and drag coefficient (ζ) of 0.55 are considered to be acceptable values in the literature and were therefore considered here as reference values ([53]). The fiber aspect ratio was set to 250 making the fiber input length as 3 mm. Thus, the relevant initial values are presented in the Table 4.2.

After running the simulation, the agreement between the experimental and the simulation was checked, and the deviation from the experimental values seemed quite apparent, as can be seen from Figure 4.3:

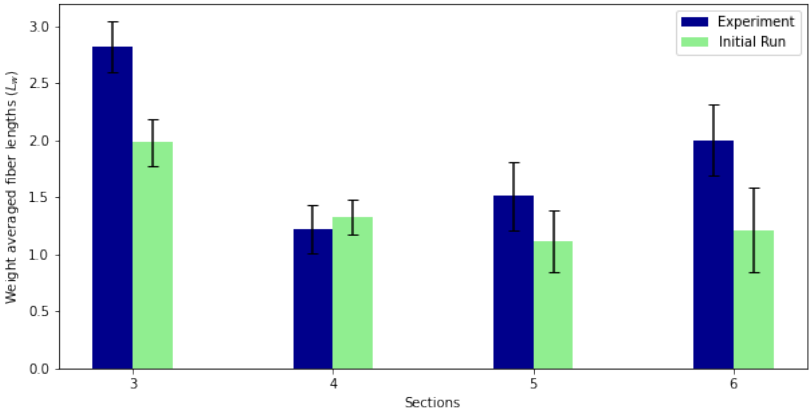

(a)

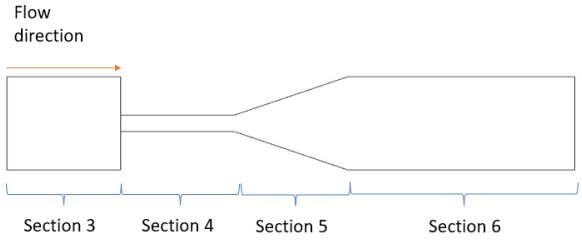

(b)

Figure 4.3: (a) Results from the initial study from the fiber breakage model in the software. (b) Insert C model with sections observed for the fiber breakage.

Since the disagreement between the first trial run and the experiments is quite considerable, a parametric study was conducted where a set of simulation runs were conducted to understand the influence of individual Phelps model parameters on the fiber breakage (Table 4.3). Parameters like fiber length and fiber diameter were kept constant and fiber length input of 3 mm was selected.

Table 4.3: Variation of the resulting weight averaged fiber lengths (L_w) with changing Phelps model parameters for performing parametric tuning.

	Fiber length (L_w) in sections (mm)			
For Drag Coefficient	3	4	5	6
$\zeta = 0.5$	2.0	1.09	1.44	1.65
$\zeta = 1$	2.01	1.08	1.43	1.67
$\zeta = 1.5$	2.02	1.13	1.48	1.69
For Breakage Coefficient	3	4	5	6
$C_B = 0.03$	2.02	1.08	1.43	1.67
$C_B = 1$	0.31	0.28	0.30	0.28
$C_B = 2$	0.29	0.28	0.27	0.28
For scalar factor	3	4	5	6
S = 0.1	1.55	0.75	1.07	1.16
S = 0.5	1.89	1.07	1.44	1.54
S = 1	2.02	1.08	1.43	1.67

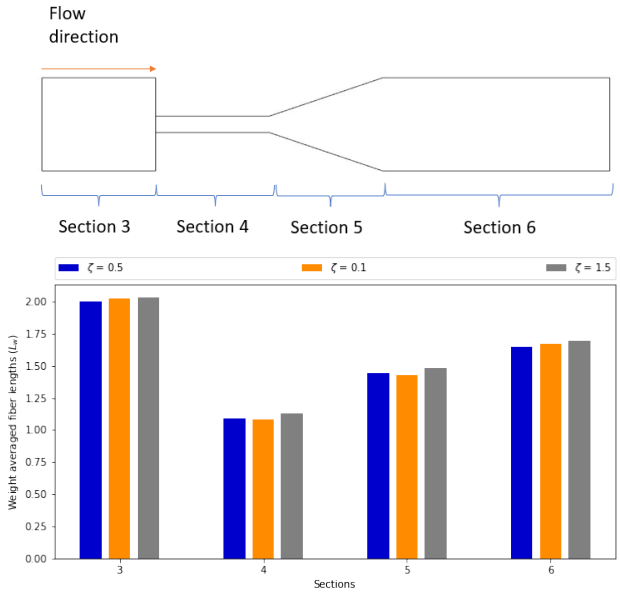

(a) Fiber breakage variation with drag coefficient

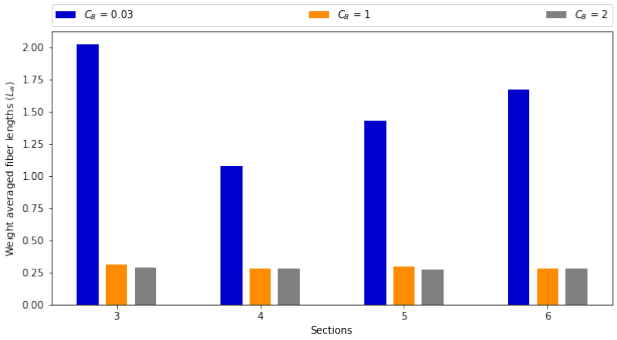

(b) Fiber breakage variation with breakage coefficient

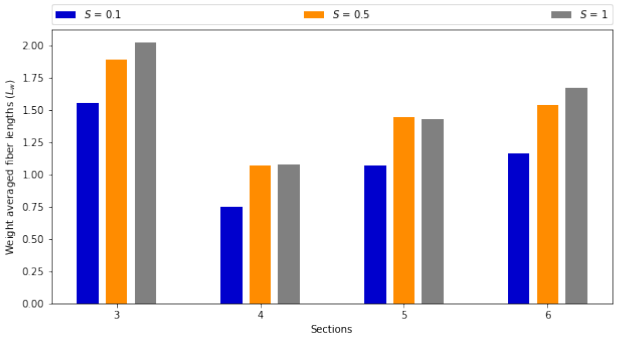

(c) Fiber breakage variation with scalar factor

Figure 4.4: Variation of the fiber length (mm) as observed with changes in the different tuning parameters of the Phelps model in the Moldex3D software.

From the plots and the table, it was observed that for increasing value of drag coefficient (ζ), a slight increase in the residual fiber length is observed, indicating that increase of drag coefficient decreases fiber attrition. For breakage coefficient (C_B), increasing value leads to higher fiber breakage, which is expected from the factor, as it controls the rate at which fibers tend to break during the process. For scalar factor (S), an increasing value of S leads to increasing value of residual fiber length, implying an inverse relation between S and fiber attrition.

Based on the observations from the parametric study of the Phelps model, the trend of fiber breakage along the geometry was tuned. However, to manage the initial length values of the plots (at part 3), the initial length needs to be adjusted as well. The check for initial fiber length was made by changing the aspect ratio in the software and keeping all the other parameters fixed. The experimental fiber length at the section 3 is approximately 2.82 mm (Table 3.1). Since, in the software, the initial length is input at part 1 (Figure 4.2), a hit and trial method is used to match the experimental and the simulated fiber lengths at part 3. The Table 4.4 shows initial fiber lengths considered at section 1 and the resulting fiber lengths at section 3, 4, 5 and 6. Further, the plot also shows the

comparison between the all the readings together with experimental results.

Table 4.4: Fiber length variation in the sections of the insert C as a function of the different initial fiber lengths considered in the study.

	Part (Fiber length (L_w) in mm)				
For fiber length (Fl)	Aspect ratio	3	4	5	6
Experimental	-	2.82	1.22	1.51	2.00
Fl = 3 mm	250	2.02	1.08	1.43	1.67
Fl = 4.25 mm	354.12	2.88	1.05	2.263	2.63
Fl = 5 mm	416.67	3.394	1.779	2.55	2.76

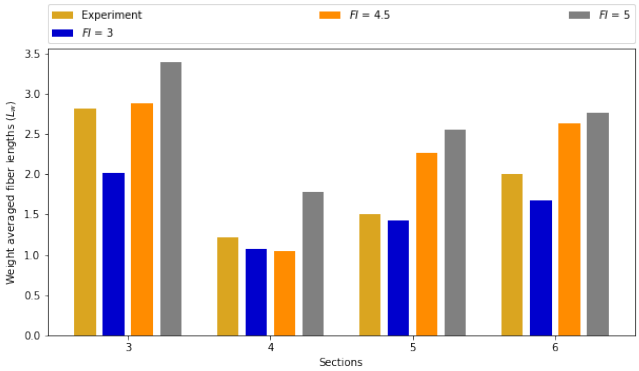

Figure 4.5: Fiber length (mm) variations as function of different input fiber lengths in the Moldex3D software.

From the readings and the plot, it can be seen that an input fiber length of 4.25 mm presents the most accurate length at section 3 with respect to the experimental data. Therefore, an input length of 4.25 mm is chosen. However, the remaining sections need to be approximated as well, and will be done by tweaking the other parameters.
Based on the observations of the parametric study, further adjustments were carried out on the parameters to predict the experimental results and after a number of trials, an acceptable fit was observed between the trials and the experimental data. This fitted curve is presented in the Figure 4.6.

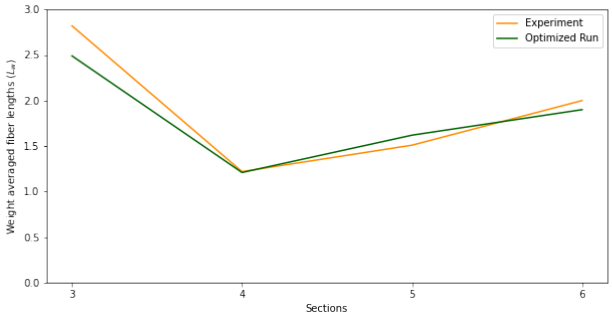

(a)

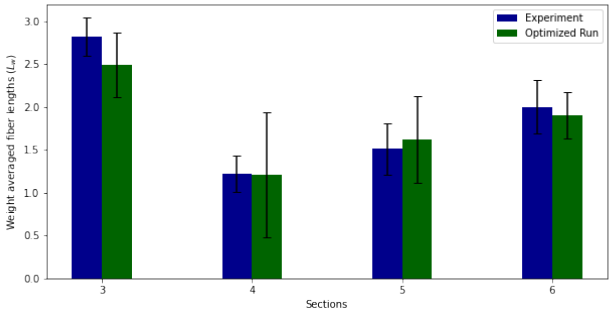

(b)

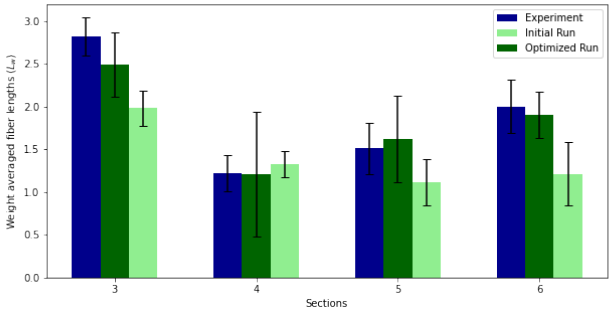

(c)

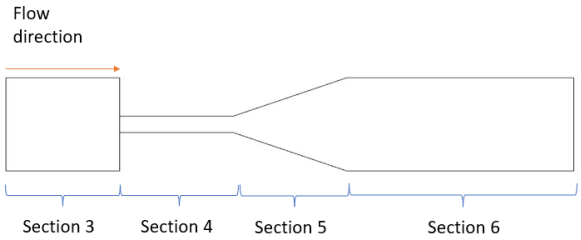

Figure 4.6: (a)&(b) Final optimized results obtained after tuning the computational Phelps model parameters as compared to the experimental runs. (c) Initial run is depicted in comparison with experimental observation and optimized run to show the difference after tuning.

From the plots, the accepted run shows very good agreement with the experimental results. It also shows great improvement in fiber breakage prediction compared to the first run.

Table 4.5: Results obtained from the simulation study in the software before and after optimization of the Phelp model parameters as compared to experimental results.

Trial	**Input**				**Output fiber lengths L_w (mm)**			
	Scalar factor (S)	**Breakage coefficient (C_B)**	**Drag coefficient (ζ)**	**Aspect ratio**	**Section 3**	**Section 4**	**Section 5**	**Section 6**
Baseline Run	1	0.03	0.55	250	1.98	1.33	1.12	1.21
Accepted Run	0.3	0.03	1	354.12	2.49	1.2	1.62	1.9
Experimental Run	-	-	-	-	2.82	1.22	1.51	2

Table 4.6: Percentage absolute errors observed as compared to the experimental runs before and after the optimization of the model parameters in the software.

Errors (%)	Section Fiber length (in mm)			
	3	4	5	6
Baseline Run	29.8	9.01	25.82	39.5
Optimized Run	11.70	1.64	7.28	5

From the errors presented, it can be safely concluded that agreeable fitting between the experimental and the simulation runs has been performed, which has been one of the primary goals of the study.

Further, to understand the influence of flow on the fiber breakage, fiber lengths obtained in the simulated geometry are presented along with the shear rates and viscosity variations (Figure 4.7). From the simulations, it can be observed that fiber lengths are directly influenced by the shear rate variations along the geometry. With high levels of shear rate, higher fiber breakage is observed, which is in accordance with the experimental studies, as higher shear rate cause more strain to the fibers leading to their breakage. This rise in shear rates is observed for zones with small cross-sectional areas. In terms of viscosity, it is observed to vary slightly more along the corners and edges as well as along the cross-sectional changes. With increasing viscosity, the fiber breakage tends to decrease. This is because along the corners, increasing viscosity reduces the drag force observed by the fibers, leading to decreased attrition and higher fiber length.

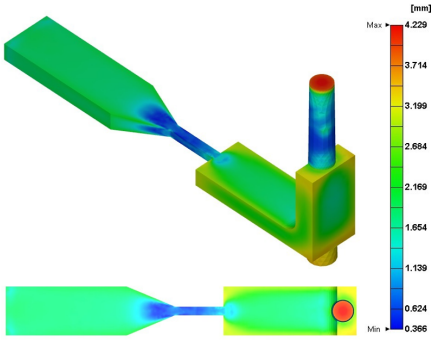

(a)

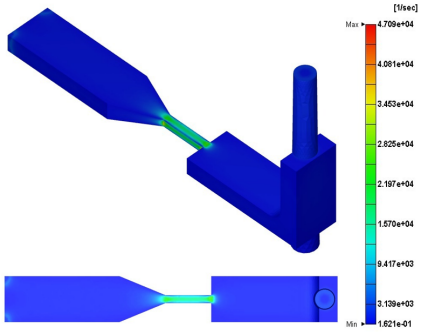

(b)

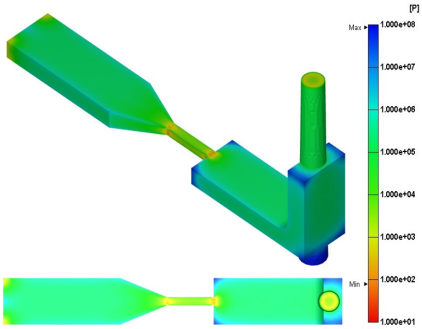

(c)

Figure 4.7: Simulation results for optimized parameters as obtained in Moldex3D software for insert C (a) Fiber lengths (b) Shear rates (c) Viscosity

It is also observed in the experiments (Figure 4.6) and the simulations (Figure 4.7), that the fiber lengths tend to decrease in the smaller orifices (section 4) and seem grow again in larger segments (section 6). This is due to the fact that fibers of larger lengths gets pushed along the flow in the smaller orifices, as they remain in the 'core' part or the centre of the flow, whereas the smaller fibers get pushed to the sides near the walls of the cavity. This observation is difficult to obtain in experiments with FLD as they only provide the averaged data of fiber lengths. They do not provide actual representation of how the fibers are distributed within the geometry. However, with simulations and models, the observation has been quite well reasoned.

To understand the degree of tuning required with the change in the geometry, the next step was to apply the model parameters obtained from the fitting of insert C to the geometry of insert A and insert B (Figure 3.4). To perform this, the model of insert A and B was developed in the Solidworks, in manner similar to that insert C.

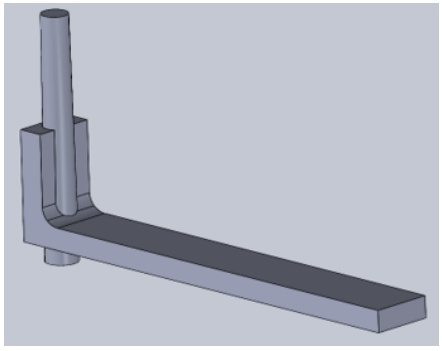

(a)

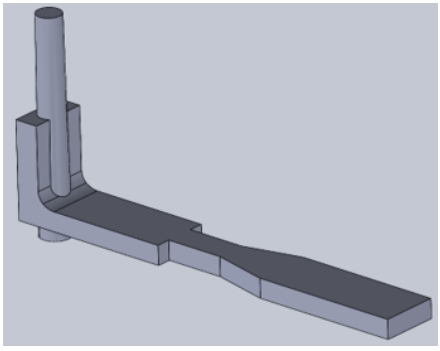

(b)

Figure 4.8: Geometrical model developed in the Solidworks for (a) Insert A (b) Insert B.

Table 4.7: Comparison of the simulated fiber lengths with the experimental fiber lengths (L_w) with the tuned parameters obtained from the fitting of Insert C.

Mold Insert	Position	Experimental fiber length (mm)	Simulated fiber length (mm)	% Error
A	1	3.43	4.06	18.37
	2	4.16	3.34	19.64
	3	3.43	2.21	35.66
	4	2.88	2.15	25.35
B	1	3.40	4.10	20.59
	2	4.79	3.42	28.71
	3	4.33	2.40	44.62
	4	2.27	2.17	4.23
	5	3.82	2.23	41.73
	6	3.51	2.22	36.75

The geometries were than imported to the Moldex3D software and all the meshing and run was developed in the similar manner as that of insert C. The input to these run were provided the same as that optimized for insert C (Table 4.5) and the results were checked.

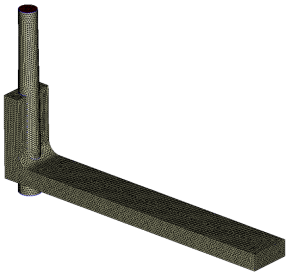

(a)

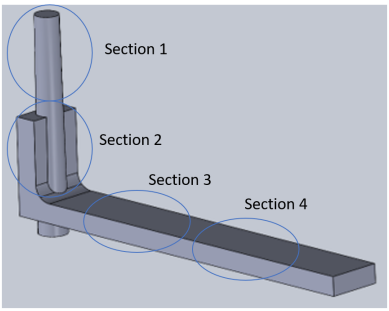

(b)

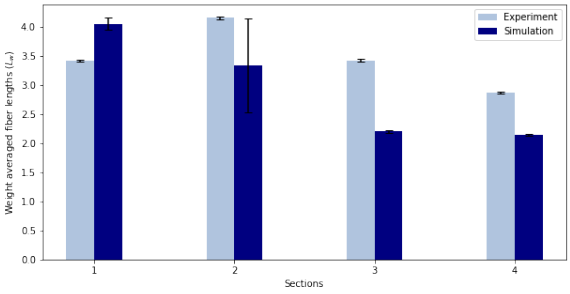

(c)

Figure 4.9: Insert A fiber lengths (L_w) as observed in the different sections obtained with tuned parameters from simulation study for insert C.

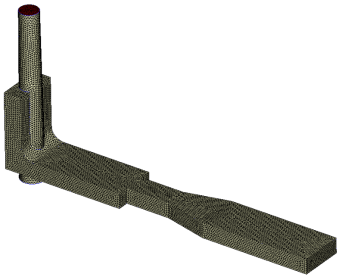

(a)

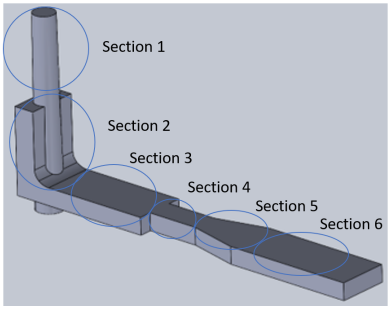

(b)

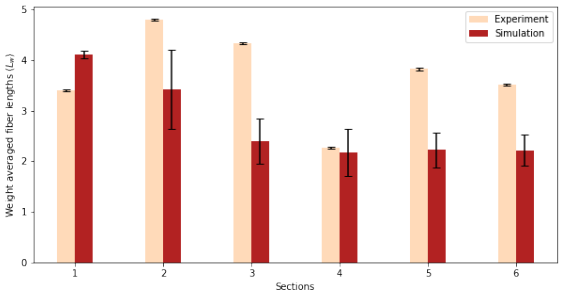

(c)

Figure 4.10: Insert B fiber lengths (L_w) as observed in the different sections obtained with tuned parameters from simulation study for insert C.

From the Table 4.7, it can be observed that the agreement for insert A and insert B, is not really good, as compared for insert C (Table 4.6) for the same inputs. The % error observed in each of the sections for the other geometries is significantly high, and can not be considered as an acceptable fit. The only agreement as observed from the plots (Figure 4.9 & Figure 4.10), is the trend between the fiber breakage, which seems to go down further down the stream, as more fiber breakage is observed. This implies that the use of software for the prediction of the fiber length is also needs to be re-tuned with change in geometry. Therefore, considerable tuning is needed for the prediction of a single output run.

The fiber breakage observed in insert A and insert B, is also shown in Figure 4.11 and Figure 4.12. Here, corresponding shear rates and viscosities are also shown. The relation between the shear rates, viscosities and fiber breakage is observed to be the same as in insert C (Figure 4.7). The fiber breakage tends to increase with increasing shear rate, whereas the fiber breakage tends to slightly decrease with increase in viscosity, usually observed along the edges and corners.

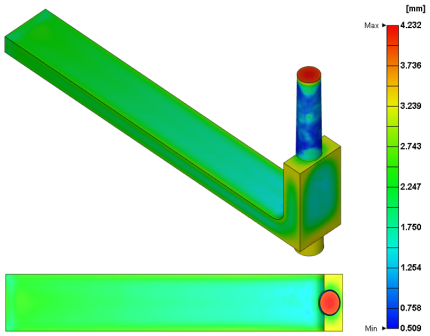

(a)

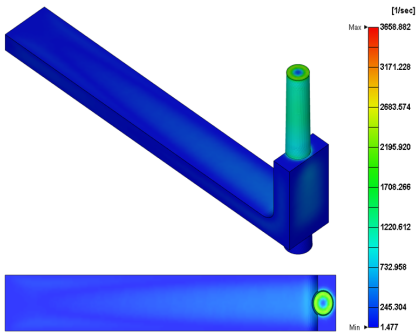

(b)

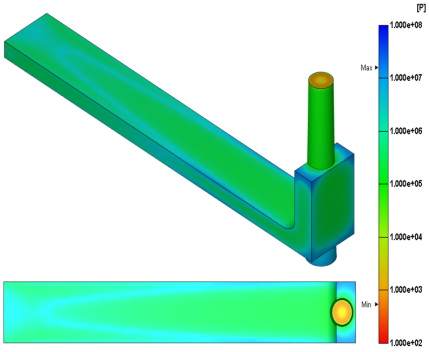

(c)

Figure 4.11: Simulation results for optimized parameters as obtained in Moldex3D software for insert A (a) Fiber lengths (b) Shear rates (c) Viscosity

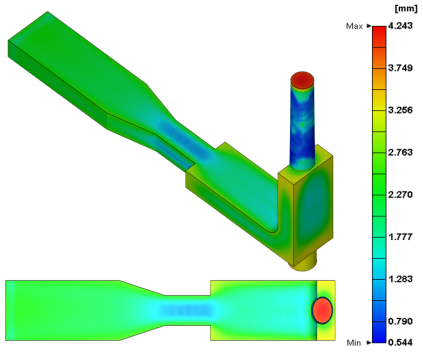

(a)

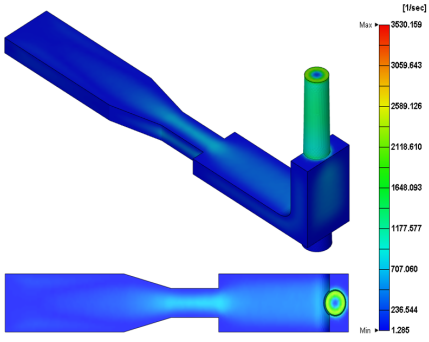

(b)

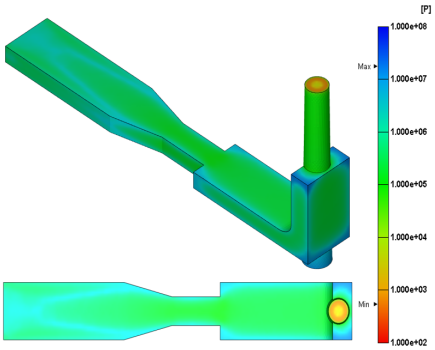

(c)

Figure 4.12: Simulation results for optimized parameters as obtained in Moldex3D software for insert B (a) Fiber lengths (b) Shear rates (c) Viscosity

4.2. ANALYTICAL RESULTS

The codes developed to perform the analytical study can be accessed here.

Based on the methodology presented in section 3.5, the analytical study was performed as a post-processor to the data obtained from the simulation of the geometrical model in Moldex3D software.

4.2.1. NODAL CONVERGENCE STUDY

To perform the application of the models as a post processor to the data, and predict the fiber breakage, first a convergence study was conducted which was used to estimate the nodal resolution needed to extract acceptable results. This means that different amount of probe nodes were created on the geometry of a simulated injection molding model in Moldex3D, and the resulting fiber lengths obtained from the MATLAB codes for the models were compared as a function of number of probe nodes.

The probe nodes were evenly distributed in each of the sections of the 'insert C' geometry, according to Figure 4.13 and the nodal positions in the geometry are presented in the Figure 4.14

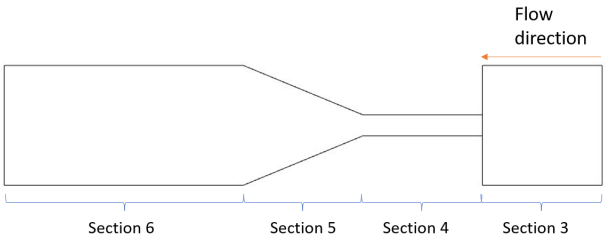

Figure 4.13: Insert C geometry with defined parts for the measurement of the fiber length distributions.

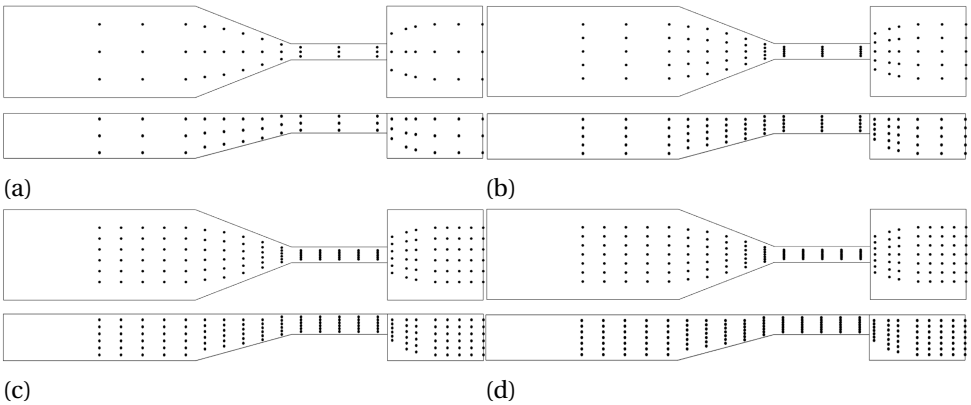

Figure 4.14: Schematics of the probes (top view and front view) distributed in the Moldex3D used for data extraction for different probe resolution. (a) 153 probes, (b) 425 probes, (c) 828 probes and (d) 1127 probes.

The fiber length was then calculated in each of the probes, and the averaged fiber length (L_w) was estimated for each of the sections. This method was performed for both, Phelps model and the Bechara model. The number of probes and the corresponding sectional fiber lengths for Phelps model are shown in the Table 4.8 and the Figure 4.15, and for the Bechara model, in the Table 4.9 and Figure 4.16

Table 4.8: Fiber lengths (L_w) observed from the different nodal resolutions along the geometry of the insert C with Phelps analytical model.

Probes	Sectioned averaged L_w (mm)			
	3	4	5	6
153	1.95	0.35	1.14	1.98
425	1.91	0.34	1.13	1.99
828	2.01	0.33	1.11	1.97
1127	2.01	0.34	1.11	1.97

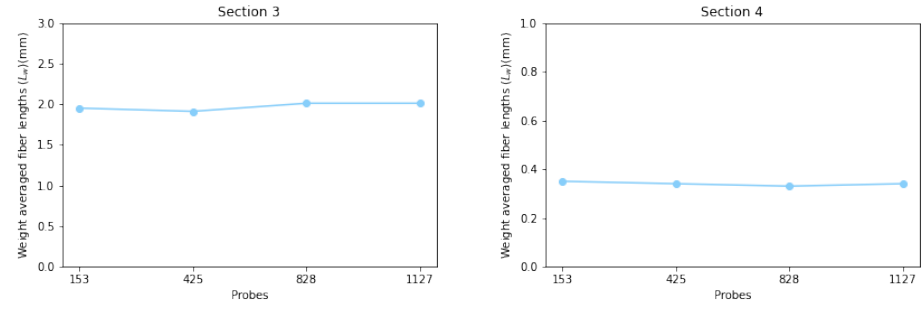

(a) (b)

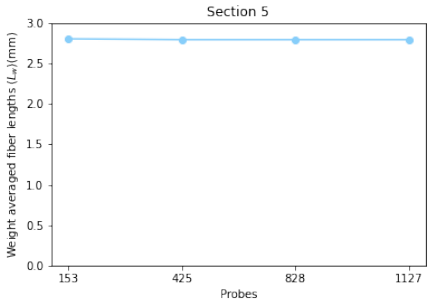

(c)

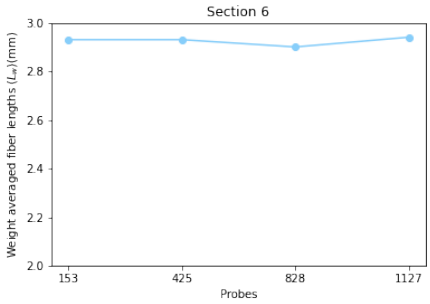

(d)

4

Figure 4.15: Convergence trends observed for weight averaged fiber lengths (L_w) along for the different sections of the insert C geometry as obtained from Phelps analytical model.

Table 4.9: Fiber lengths (L_w) observed from the different nodal resolutions along the geometry of the insert C with Bechara analytical model.

Probes	Sectioned averaged L_w (mm)			
	3	4	5	6
153	2.89	2.40	2.80	2.93
425	2.87	2.39	2.79	2.93
828	2.89	2.40	2.79	2.94
1127	2.88	2.40	2.79	2.94

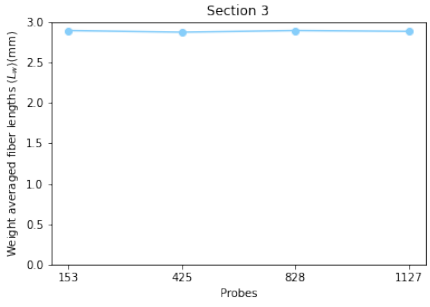

(a)

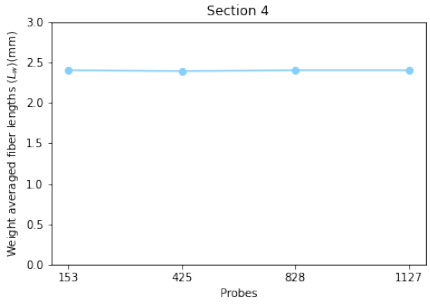

(b)

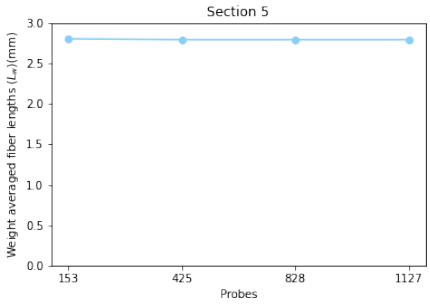

(c)

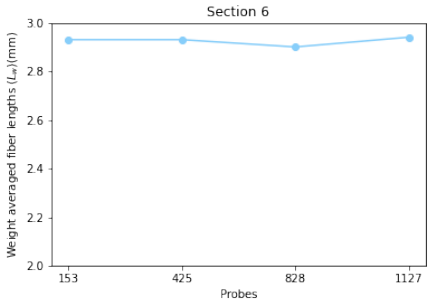

(d)

Figure 4.16: Convergence trends observed for weight averaged fiber lengths (L_w) along for the different sections of the insert C geometry as obtained from Bechara analytical model.

From the results obtained, it can be seen that the values of the fiber lengths obtained from the increasing nodal resolutions are relatively close, with maximum deviation of about 8% in Phelps convergence data and about 3% in Bechara convergence data, when difference between the extreme values of any given section were considered with varying probes. Therefore, with the convergence results, it can be concluded that the models provide agreeable results with even less number of probe points.

4.2.2. PHELPS ANALYTICAL MODEL

After the convergence test was performed, analysis of the Phelps MATLAB code was conducted, by comparing it to the results obtained from fiber breakage in simulation in Moldex3D. The Phelps analytical model is compared with the Moldex3D for the different nodal resolutions. The results are obtained for similar input conditions, model parameters and material properties. These are presented in the Table 4.10 and the results are presented in the Figure 4.17.

Table 4.10: Input parameters for Phelps analytical model

Parameter	Value
Initial fiber length (μm)	3
Drag coefficient (ζ)	3
Breakage coefficient (C_B)	0.02
Scalar factor (S)	0.25

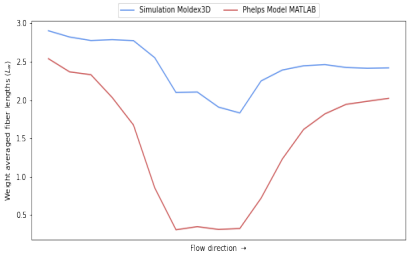

(a)

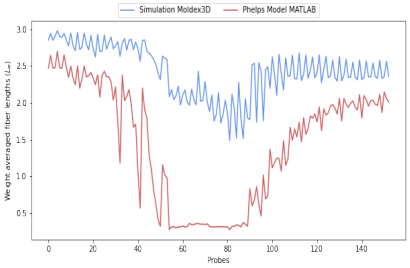

(b)

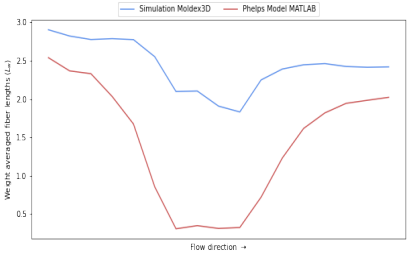

(c)

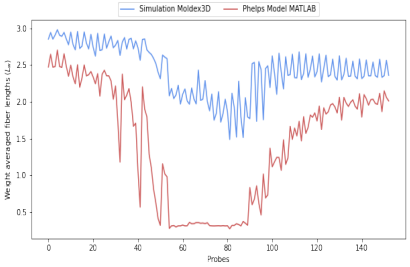

(d)

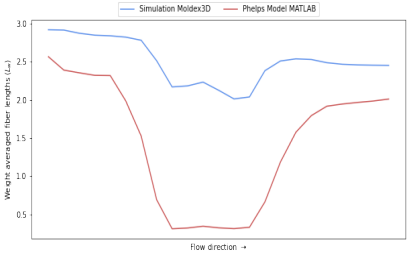

(e)

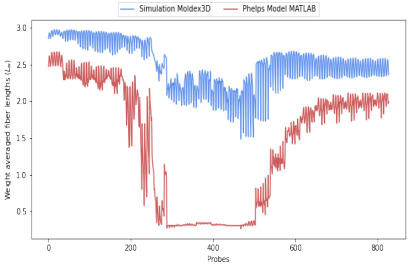

(f)

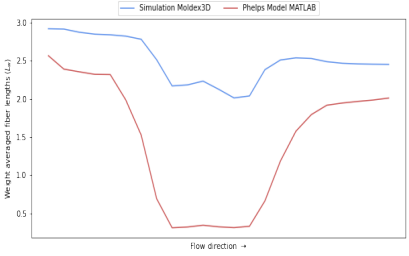

(g)

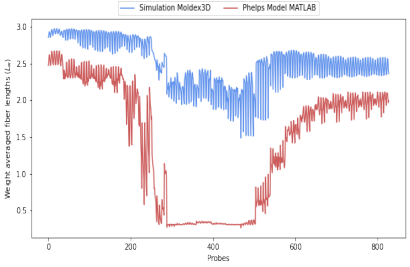

(h)

Figure 4.17: Fiber lengths trend observed with sections and corresponding probes between Moldex3D software and analytical Phelps model for different probe resolution. (a) and (b) 153 probes, (c) and (d) 425 probes, (e) and (f) 575 probes, and (g) and (h) 1127 probes.

From the plots, it can be observed that Phelps model developed through analytical MATLAB code, predicts quite well in terms of the trends of the fiber breakage observed in the simulation. However, the MATLAB code clearly under predicts residual fiber lengths, or in other words, it over predicts the breakage as compared to the simulations. The possible reasons for this over prediction of breakage are listed as follows:

- The model applied in the MATLAB code is a pure Phelps model, without any effect of fiber orientation, concentration or flow rheology influence. However, the Moldex3D software also involves some other parameters or models to predict orientation and concentrations of fiber in the whole cavity during filling. This could perhaps influence the residual fiber lengths results as well.
- Another possible cause of difference in the results could be the FEM method applied in the code as compared to the software. The code applies a layered nodal discretization, where each node connects to the previous node in the same layer of the same axis direction (this has been explained in subsection 3.5.3). The software perhaps could have applied a different FEM approach for the fiber length prediction at each node over period of time. This could lead to a fundamental difference between the two results.
- the nodal resolution could also be the cause for the difference in the accuracy of the results. Perhaps with more nodal resolution, fiber breakage trend may become more agreeable.

The analytical Phelps model does not give accurate fiber length values for the nodal data, compared to the Moldex3D simulations. However, it does predict the trend of the fiber lengths in the geometry quite well. To check this further, a through thickness fiber length variation is obtained from the Phelps model and the Moldex3D simulation. Here, fiber length variation along the thickness of a given section is compared to the simulation.

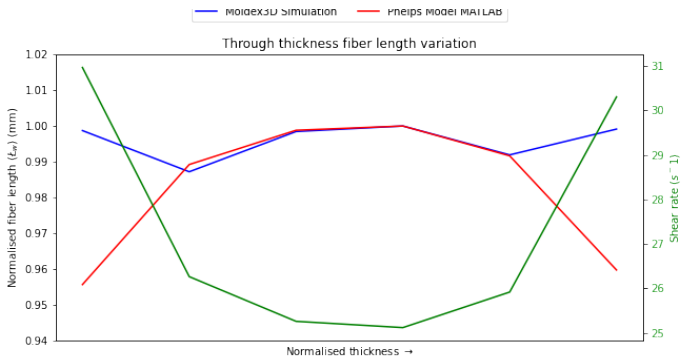

Figure 4.18: Normalised through the thickness fiber variation as observed Phelps analytical model and Moldex3D simulations, along with variation in shear rate for insert C

As observed from the Figure 4.18, the fiber length variation is quite well predicted by the Phelps analytical model through the thickness as compared to the Moldex3D simulations, apart from near the edges. This is because, the Moldex3D implements 'fountain flow' method of flow front, where the fibers in the melt front are deposited near the walls in the next time step. In this work, this method of melt flow is not incorporated, which could be another reason for observed variations in fiber lengths value predicted. The lengths are normalised as the purpose of this comparison is to establish the accuracy in predicting the variation. Further, the result also validates the trend that increasing fiber breakage is observed with increasing shear rates, even in the local regime of thickness variation, and the longer fibers are obtained in the central core region of the cavity during filling.

4.2.3. BECHARA ANALYTICAL MODEL

After the Phelps analytical model, the Bechara analytical model was also developed in the MATLAB and applied to the same geometry with similar rheological results as obtained from Moldex3D. The inputs delivered to the model as model parameters are presented in the Table 4.11. The fitting parameters have been chosen based on the work performed in [59], since the materials used are the same.

Table 4.11: Input parameters for Bechara analytical model

Parameter	Value
Initial fiber length (μm)	3
Fiber interaction factor (λ)	0.085
Breakage rate coefficient (ξ)	12.1×10^{-4}

Again, for the Bechara model, the nodal resolution was incremented, and the fiber breakage trends were calculated and compared to the software results. The results are presented in the Figure 4.19.

As observed from the results, the Bechara model also predicts the trend quite well in comparison with the moldex3d simulations obtained in the Figure 4.19. However, it seems to slightly under predict the breakage of the fibers all of the sections, especially in the final part of the geometry. During the final part of the geometry, the fiber length trend is expected to decrease, however, in the analytical model, it observed to rise until a steady value. The reason for this could be the FEM method applied in the analytical model. This can, however, be controlled with a better tuning of the fitting parameters, and perhaps can be used to fit to the experimental results.

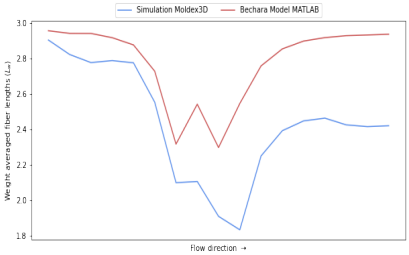

(a)

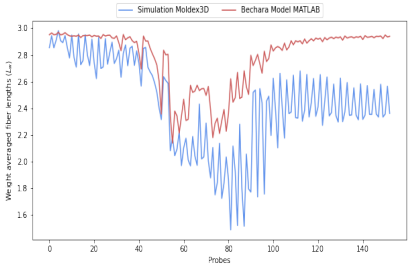

(b)

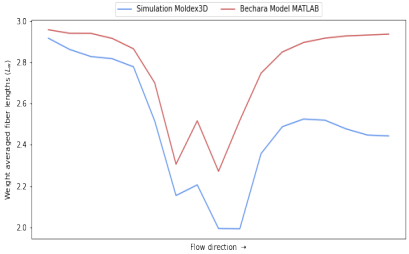

(c)

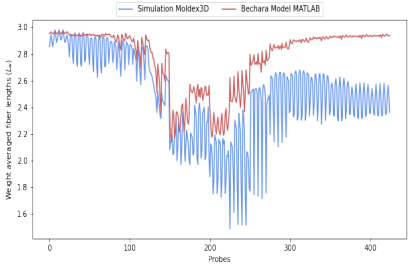

(d)

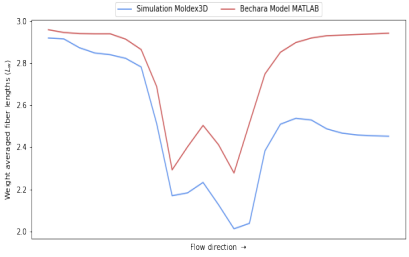

(e)

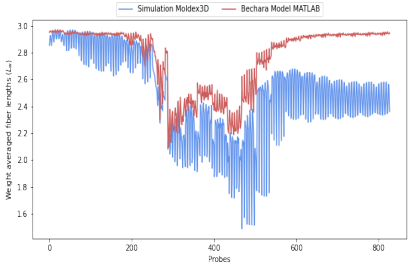

(f)

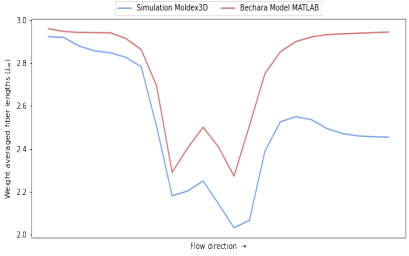

(g)

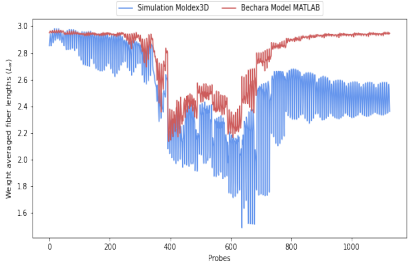

(h)

Figure 4.19: Fiber lengths trend observed with sections and corresponding probes between Moldex3D software and analytical Bechara model for different probe resolution. (a) and (b) 153 probes, (c) and (d) 425 probes, (e) and (f) 575 probes, and (g) and (h) 1127 probes,

After establishing the implementation of the two models as post-processors to the simulation software, the models were then compared together with Moldex3D results and the obtained trends for the two models are presented in the Figure 4.20.

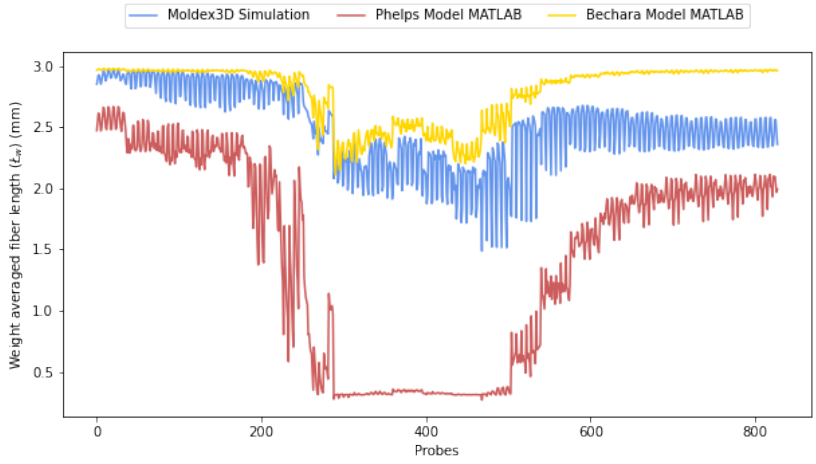

(a)

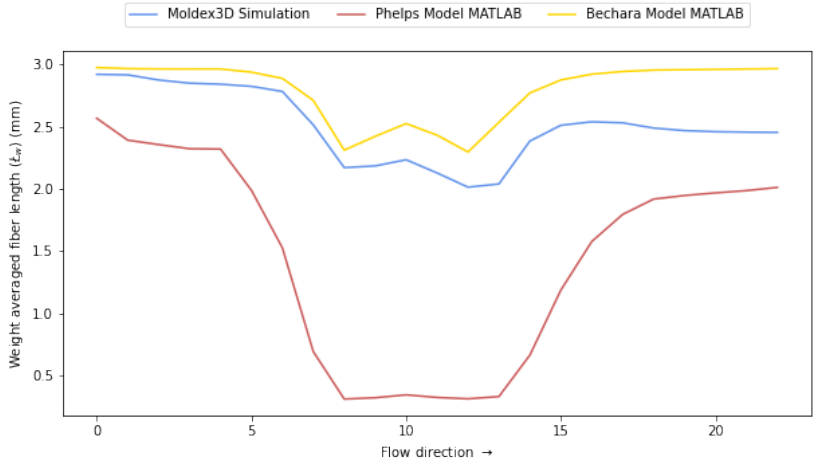

(b)

Figure 4.20: Comparative prediction between Moldex3D, Phelps model and Bechara model for fiber lengths (L_w). (a) Comparison between corresponding probes, (b) Comparison between sections.

As can be seen from the results, both of the models predict the general trend for breakage quite well as compared to the results, however, there is still a need for signifi-

cant amount of parameter tuning for each of the model to get proper fitted results to the Moldex3D.

To compare the prediction accuracy of the two models with experimental data, the fiber lengths distribution obtained from the experiments (Table 3.1) have been compared to the FLDs predicted using the models. The Phelps model involves the calculation of the fiber length distribution at every node. Therefore, to calculate the fiber length distribution of a section to compare with the distribution observed in the experiments, all the nodal distributions are averaged corresponding to that section. Further, since exact distribution input at the experiment is not known, this could create a difference in the two estimations. Thus, the results are calculated as normalised values. For Bechara model, the calculation of averaged fiber lengths are done directly without the estimation of the fiber length distributions at nodes. Therefore, the fiber length distribution is calculated using the number averaged (L_n) and weight averaged (L_w) fiber lengths as the moment for a lognormal probability density function as suggested in literature ([59]) given by the Equation 4.1:

$$f(x) = \frac{1}{x\sigma\sqrt{2\pi}} \exp\left(\frac{(\ln x - \mu)^2}{2\sigma^2}\right) \tag{4.1}$$

With the distributions obtained for each of the sections, they are plotted together in the Figure 4.21.

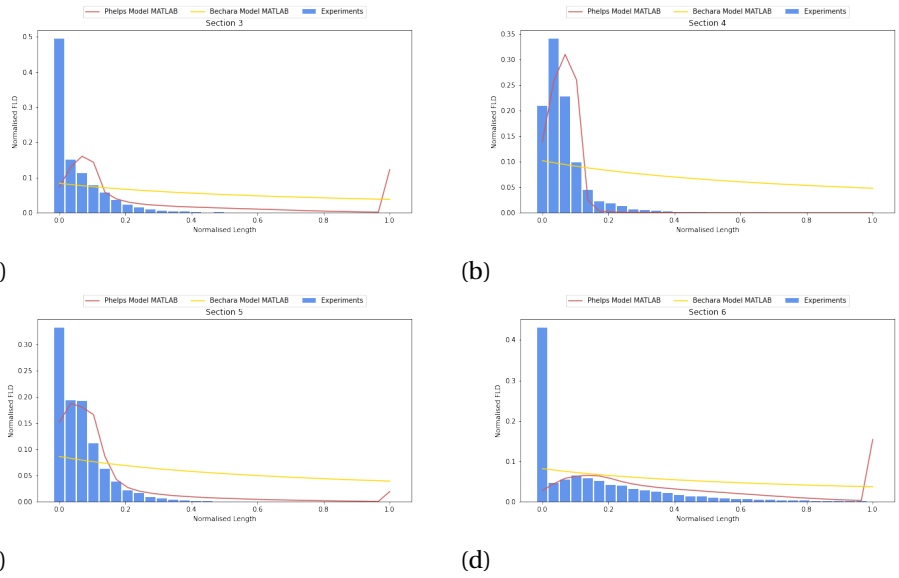

Figure 4.21: Normalised FLD comparisons for Experiments, Phelps model and Bechara model at sections (a) 3 (b) 4 (c) 5 (d) 6.

From the figure, it can be observed that Phelps model provides a relatively better agreement to the trend observed in the experiments as compared to Bechara model,

which completely fails to capture the experimental observations. Apart from the fiber length distributions, cumulative fiber lengths distributions or geodesic FLDs for each of the models are also calculated together with the experimental data. This data is again normalised, and presented in Figure 4.22

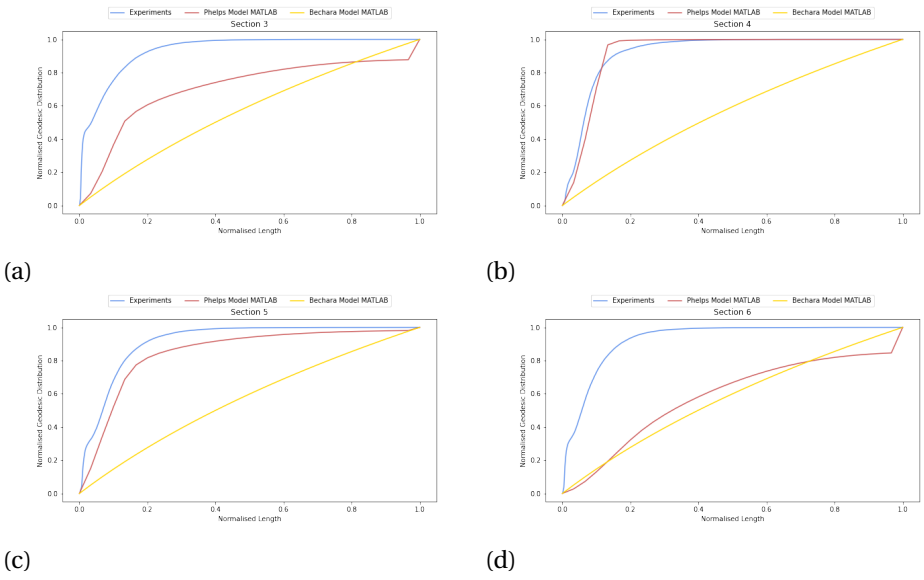

Figure 4.22: Normalised geodesic FLD comparisons for Experiments, Phelps model and Bechara model at sections (a) 3 (b) 4 (c) 5 (d) 6.

Again, the results show that the Phelps model captures a better distribution (except section 6) of the fiber lengths as compared to the Bechara model. Therefore, it can be claimed that the fiber length distribution obtained from the Bechara, may not be the best method, and perhaps some other distributions can be considered instead of lognormal PDFs.

A recommendation for choosing Schulz-Flory distribution (SFD) is proposed in this work. It is a distribution which aims to describe the relative ratios of polymers of varying lengths (monomer units) occurring in a step-growth polymerisation process. This means that weight average molecular weight distribution of the polymers can be calculated using the SFD which is given by Equation 4.2.

$$w_x = x(1-p)^2 p^{x-1} \tag{4.2}$$

Here, w_x represents the weight fraction (or mass fraction) of a given polymer with x monomer units. p represents the fraction of the reacted monomer units, and is an empirically determined value to represent the distribution with a value ranging between $0 < p < 1$. The choice for SFD over the lognormal distribution in the Bechara model seems more reasonable based on the fact that discretization of a fiber into small 'monomers' of smaller fiber lengths makes a valid foundation for the distribution model. Further, the

'polymerisation' effect of the SFD can also be considered as 'breakage' or 'de-polymerisation' effect with simply reversing the value of p in the Equation 4.2. In the Equation 4.2, w_x represents the weight fraction which corresponds to the number of 'x' monomer units, this can be also interpreted as a relation between the fiber count and the length of a given fiber. With this hypothesis, the SFD was then applied to experimental data with the value of x assumed to be the smallest resolution of the fiber length is used in the analytical models, and the p manually adjusted for a good fit.

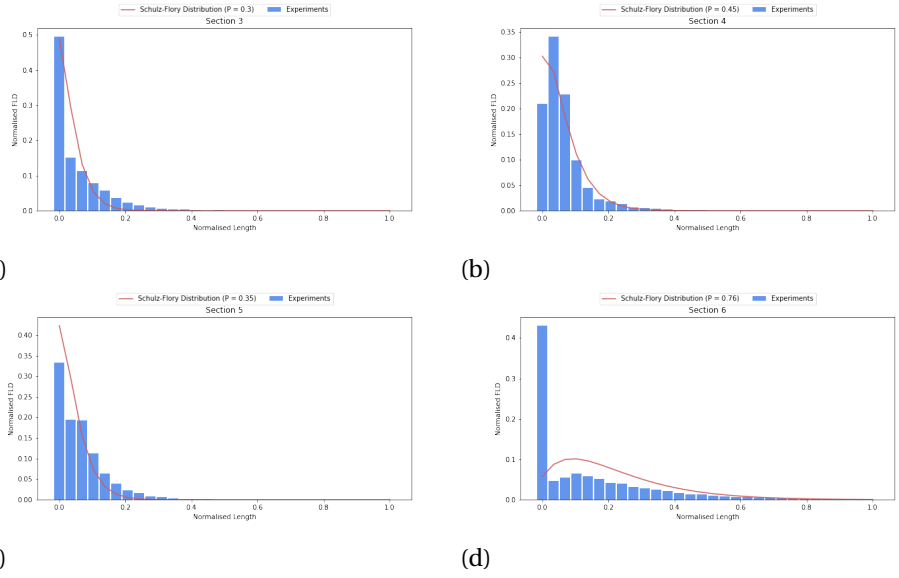

Figure 4.23: Normalised FLD comparisons for Experiments and SFD at sections (a) 3 (b) 4 (c) 5 (d) 6.

From the Figure 4.23, it can be observed that the SFD certainly provides as better fit to the experimental data as compared to the Bechara model predictions in Figure 4.21 using lognormal PDF. It can be noted that it fails to capture the initial rise in the FLD in section 4 and also it tends to over predict in the smaller fiber lengths for sections 3, 5 and 6. To avoid this, it is suggested to further improve the parameter tuning of the model. Regardless, the SFD model seems to be a better option than lognormal PDF as it is based on the concept of polymerisation, and can be transferred to fiber breakage with slightly redefining the parameters.

4.2.4. MODELS REVIEW

Based on the analytical results observed until here, a comparative review the models is presented discussing the roots of similarities and the differences in the results. A scope for modification of the two models is also proposed to progress for the future works.

Although, both of the models provide similar trends, the values of the fiber lengths obtained in the two models are quite different. This is due to the inherent difference

between the two model owing to the breakage mechanism considered for fiber attrition (Equation 3.5 & Equation 3.10). While the two equations contains similar terms of flow ($\dot{\gamma}$ & η_m), they assign different weights to them, with Bechara model providing certain more weight, as denoted in the exponent of $\frac{1}{2}$ as compared to $\frac{1}{4}$. The breakage mechanisms assumed to derive the unbreakable lengths in these equations, are also different, where Bechara model considers bending breakage involving ultimate tensile strength of the fiber, whereas, Phelps model involves buckling failure involving the Young's modulus. These two properties vary significantly in terms of the magnitude, and this in turn leads to difference in the fiber breakage values.

For the fitting parameters, both of the models scale breakage to shear rate as observed from the Equation 3.11 and Equation 3.6. Also, the range of these fitting parameters are similar with ξ falling in $(1 \times 10^{-3} - 4 \times 10^{-4})$ and C_B falling in the range of $(2 \times 10^{-2} - 2 \times 10^{-2})$, as suggested in the literature ([53], [59]). Therefore, with similar range of these parameters, fiber breakage observed should also be similar. This is indeed the case as observed in the Figure 4.24.

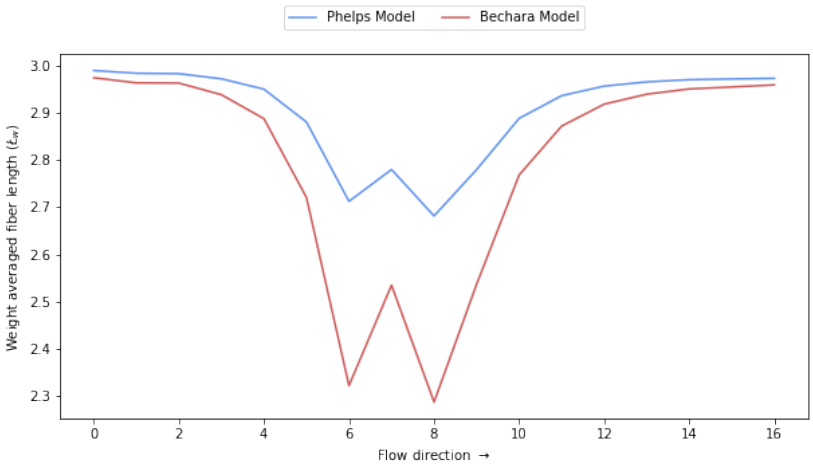

Figure 4.24: Comparison between fiber length prediction for sections between Phelps model and Bechara model for similar input of the fitting parameters, C_B for Phelps model and ξ for Bechara model.

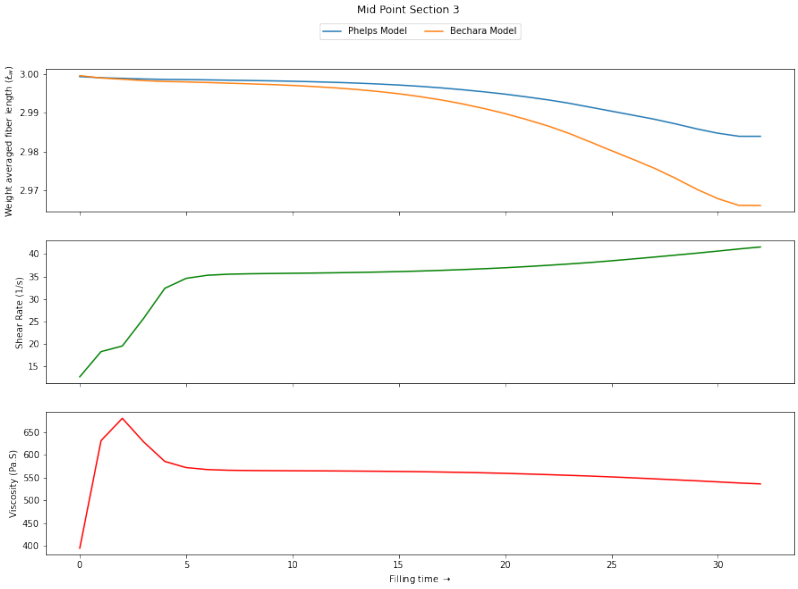

(a)

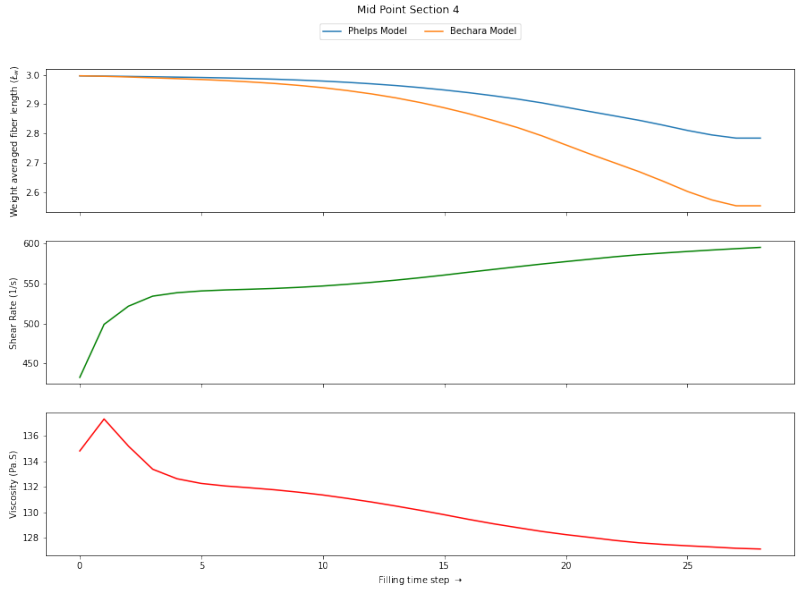

(b)

It can be seen that with same coefficient for breakage rate considered, the trends be-

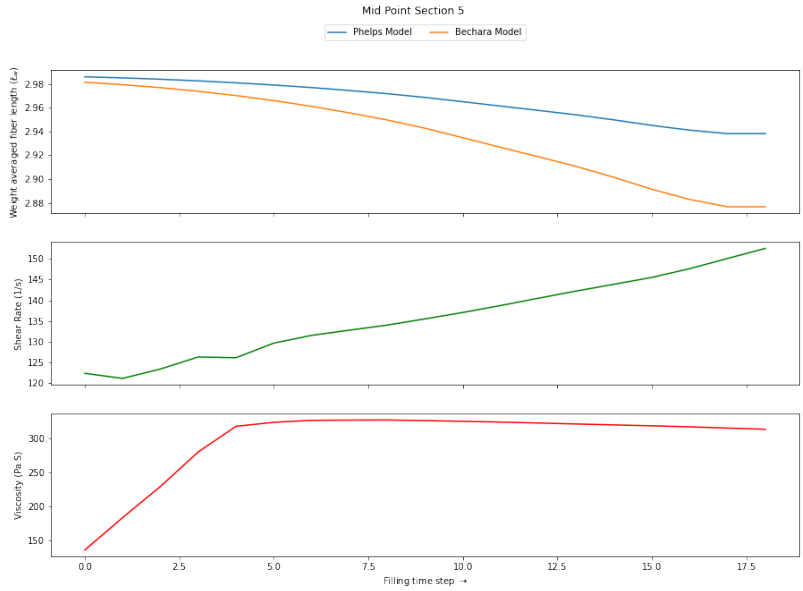
Mid Point Section 5
Phelps Model
Bechara Model
Weight averaged fiber length (lw)
Shear Rate (1/s)
Viscosity (Pa S)
Filling time step →

(c)

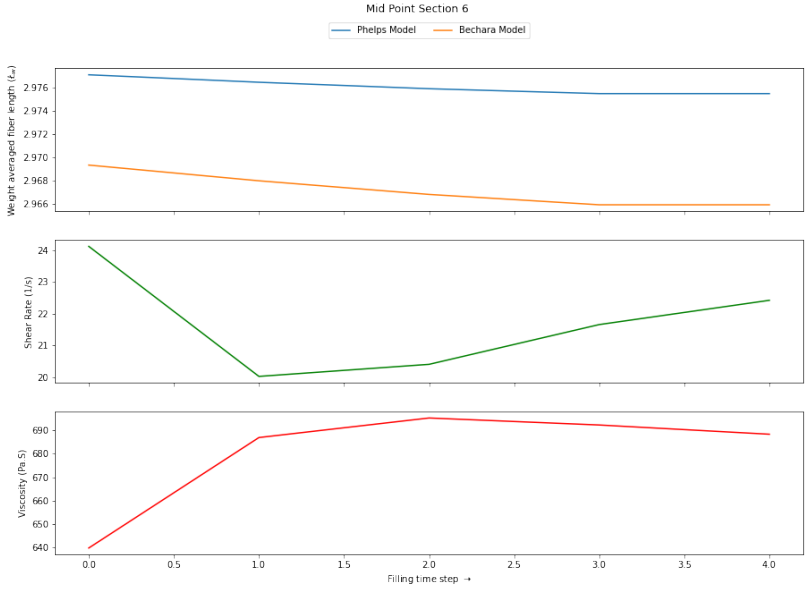
Mid Point Section 6
Phelps Model
Bechara Model
Weight averaged fiber length (lw)
Shear Rate (1/s)
Viscosity (Pa S)
Filling time step →

(d)

Figure 4.25: Fiber lengths evolution as predicted by the Phelps and Bechara model for the mid points of sections (a) 3,(b) 4,(c) 5 and (d) 6 of the insert C geometry, with same viscosity and shear rate inputs.

tween the two models become even more aligned, with Bechara model showing higher fiber breakage. This difference arises from the unbreakable length equation itself and the effect of this equation is understood by calculating breakage in the individual nodes over time, as presented in the Figure 4.25. This shows that Bechara model suffers higher breakage owing to the tensile breakage criterion considered, as compared to buckling in Phelps model.

Among the two models, in terms of computational capabilities, the Bechara model is significantly much faster as compared to the Phelps model. This is attributed to the fact that Phelp model computes the averaged fiber lengths (L_n & L_w) from the fiber length distribution for each node. This involves significantly higher computational time as compared to direct calculation of the L_n and L_w as proposed in Bechara model.

The two models seem to provide a good results for fiber breakage and are computationally feasible. While Phelps model is already incorporated into commercial fiber breakage simulation softwares, Bechara model does present itself as a potential prospect as well. However, there is still a gap in the frameworks of the two models that needs to be addressed. While Phelps model completely ignores fiber-fiber and fiber-wall interaction as mechanism for fiber breakage, using only hydrodynamic buckling failure, Bechara model tries to incorporate the fiber-fiber and fiber-wall interaction mechanism using a fitting parameter. This still fails to grasp an explicit influence of the fiber interaction mechanisms, as they are treated as a tuned parameters in a black box. Therefore, a recommendation is proposed to improve or modify the basic unbreakable length equation derived in each of the models based on a more comprehensive failure mechanism rather then only fiber buckling or fiber tensile failure. This could be done by incorporating fiber concentration into the model studies, as it may provide a better standard to incorporate fiber-fiber interaction. For fiber-wall interaction, the information of the mold geometry or the nodal locations for fiber breakage calculation would be needed to create a robust framework. Although, this is possible to be done, it would still require more research on the current foundations.

5

CONCLUSION

In this section, the conclusions obtained for the research challenges presented in the section 2.4, have been presented followed by the future recommendations to continue this study.

- **Influence of the geometry on the fiber breakage by understanding the variation in the rheology properties to propose guidelines to the designers in the industries.**
  The results for a relatively complex geometry as compared to geometries used in currently existing studies have been obtained. The fiber breakage has been successfully tuned to the experimental results for the geometry, and in comparison with the rheology properties, shear rates and viscosity have proven to show direct influence on the fiber breakage in the simulations. Higher shear rates have shown to lead to more fiber breakage, whereas higher viscosity lead to slight decrement in fiber breakage. Further, fiber breakage variations are more prominent in the edges or corners of the geometries as well as in the sections with cross-sectional changes. Locations with small cross-sectional areas are shown to have higher fiber breakage. With these observations, recommendation is made to the designers to avoid sudden changes in geometry and small cross-sections, to maintain consistency in the fiber lengths of the final product, and in turn, maintain its quality.

- **Evaluation of the Phelps model in the commercial software for predicting fiber breakage in terms of tuning required with change in geometries.**
  The Phelps model integrated in the Moldex3D software has been successfully tuned for one of the geometries to the experimental data (Insert C), with required parametric studies. Further, the tuned model has been transferred to the other geometries, insert A and insert B (Figure 3.4). The results showed that further tuning is required for the other geometries individually to properly predict the accurate fiber breakage trends along the different zones, even though the breakage trends were predict with certain accuracy. This shows that currently developed softwares

with integrated fiber breakage models still need a lot of work to improve the prediction capabilities to avoid case dependent tuning of parameters and make the simulations process much faster and accurate to avoid computational times associated.

- **Comparative study of the Phelps model with a novel Bechara model through analytical modelling to understand and benchmark the models and propose possible modifications.**
  The Phelps and the Bechara model have been successfully implemented to the Moldex3D software data as post-processors for a 3D geometrical samples, and the models predict fiber breakage trends quite well as compared to the software prediction. The models have shown similar prediction trend due to similarities in the frameworks arising from the breakage rate coefficient and the fiber unbreakable lengths considered. The two models show differences in the prediction of the fiber breakage over time, where Bechara model makes a more direct approach by calculating averaged fiber lengths (L_w or L_n) over time, whereas the Phelps model first calculates the evolution of FLD and then derives average fiber lengths. This makes Bechara model much faster with no significant loss in accuracy of the results. It also provides an equation for prediction of FLD using lognormal PDF based on averaged fiber lengths, however, it required further tuning. Another, distribution model was proposed, Schulz Flory distribution, which proved to provide better FLD prediction as compared to Bechara prediction using lognormal PDF.

5.1. FUTURE RECOMMENDATIONS

The future recommendation for the work to use this research as basis are as follows:

- The simulation studies conducted in this work can be further improved by evaluating the accuracy and tuning needed for more complicated geometries and understanding the influence of other filling parameters such as temperatures and pressure.
- The study currently addresses the fiber breakage models as independently applied to the software as post-processor. Perhaps, models for other fiber properties such as fiber orientation and concentration can also be developed and compared in conjunction to the fiber breakage models to make the models more robust and comprehensive.
- The lack of a proper model that incorporates all the breakage mechanism, i.e. fiber-melt, fiber-fiber and fiber-wall interaction also provides a scope for further work to develop a more robust model based on the current work. An unbreakable length equation derived from failure mechanisms using all three mechanisms can be used and further studied.
- The Bechara model is relatively new model, and has not been applied in the softwares, therefore future researchers are highly recommended to improve the code and work on the implementation of the model, as it has proven to be computationally time efficient.

- The fiber length distributions as observed in the models can be further improved, specifically for Bechara model, by considering Schulz Flory distribution (SFD) as a suitable alternative. SFD is defines the fraction of polymers of a given a length in a group of polymers of different lengths undergoing polymerisation. This provides a distribution similar to Phelps FLD, can be further studied.
- The analytical models used in this work can also be used to fit to the experimental data, and further assess the quality of prediction and compare to the simulation prediction, to address the computational time and cost saved.
- The study conducted in this work could also be extended to different materials, such as recycled LFTs as they tend to have slight varying initial fiber lengths. Thus, it would be interesting to study the fiber breakage and consecutive mechanical properties observed.

BIBLIOGRAPHY

[1] H. Ning, N. Lu, A. A. Hassen, K. Chawla, M. Selim, and S. Pillay, "A review of long fibre thermoplastic (lft) composites," *International Materials Reviews*, vol. 65, no. 3, pp. 164–188, 2020.

[2] J. Markarian, "Long fibre reinforced thermoplastics continue growth in automotive," *Plastics, Additives and Compounding*, vol. 9, no. 2, pp. 20–24, 2007.

[3] C. Unterweger, T. Mayrhofer, F. Piana, *et al.*, "Impact of fiber length and fiber content on the mechanical properties and electrical conductivity of short carbon fiber reinforced polypropylene composites," *Composites Science and Technology*, vol. 188, p. 107 998, 2020, ISSN: 0266-3538. DOI: https://doi.org/10.1016/j.compscitech.2020.107998. [Online]. Available: https://www.sciencedirect.com/science/article/pii/S0266353819320500.

[4] F. Rezaei, R. Yunus, and N. Ibrahim, "Effect of fiber length on thermomechanical properties of short carbon fiber reinforced polypropylene composites," *Materials Design*, vol. 30, no. 2, pp. 260–263, 2009, ISSN: 0261-3069. DOI: https://doi.org/10.1016/j.matdes.2008.05.005. [Online]. Available: https://www.sciencedirect.com/science/article/pii/S0261306908001751.

[5] M. Kazemi, S. Faisal Kabir, and E. H. Fini, "State of the art in recycling waste thermoplastics and thermosets and their applications in construction," *Resources, Conservation and Recycling*, vol. 174, no. June, p. 105 776, 2021, ISSN: 18790658. DOI: 10.1016/j.resconrec.2021.105776. [Online]. Available: https://doi.org/10.1016/j.resconrec.2021.105776.

[6] J.-P. Pascault, H. Sautereau, J. Verdu, and R. J. Williams, *Thermosetting polymers*. CRC press, 2002.

[7] S. D. A. Sharuddin, F. Abnisa, W. M. A. W. Daud, and M. K. Aroua, "A review on pyrolysis of plastic wastes," *Energy conversion and management*, vol. 115, pp. 308–326, 2016.

[8] C. Thermoplastics, "FIBER-REINFORCED POLYMER COMPOSITES," pp. 1–15, 2012.

[9] U. K. Vaidya and K. K. Chawla, "Processing of fibre reinforced thermoplastic composites," *International Materials Reviews*, vol. 53, no. 4, pp. 185–218, 2008, ISSN: 09506608. DOI: 10.1179/174328008X325223.

[10] G. Jogur, A. Nawaz Khan, A. Das, P. Mahajan, and R. Alagirusamy, "Impact properties of thermoplastic composites," *Textile Progress*, vol. 50, no. 3, pp. 109–183, 2018, ISSN: 17542278. DOI: 10.1080/00405167.2018.1563369. [Online]. Available: https://doi.org/10.1080/00405167.2018.1563369.

[11] S. Waghmare, S. Shelare, K. Aglawe, and P. Khope, "A mini review on fibre reinforced polymer composites," *Materials Today: Proceedings*, vol. 54, pp. 682–689, 2022, ISSN: 22147853. DOI: 10.1016/j.matpr.2021.10.379.

[12] U. Vaidya and K. Chawla, "Processing of fibre reinforced thermoplastic composites," *International Materials Reviews*, vol. 53, no. 4, pp. 185–218, 2008.

[13] K. K. Basumatary, "Investigation into Mechanical and Tribological Properties of Ipomoea carnea Reinforced Epoxy Composite," no. 211, pp. 1–91, 2013.

[14] Q. Zhang, Y. Liang, and S. B. Warner, "Partial carbonization of aramid fibers," *Journal of Polymer Science Part B: Polymer Physics*, vol. 32, no. 13, pp. 2207–2220, 1994.

[15] D. Jagadeesh, K. Kanny, and K. Prashantha, "A review on research and development of green composites from plant protein-based polymers," *Polymer Composites*, vol. 38, no. 8, pp. 1504–1518, 2017.

[16] T. Singh, "Optimum design based on fabricated natural fiber reinforced automotive brake friction composites using hybrid critic-mew approach," *Journal of Materials Research and Technology*, vol. 14, pp. 81–92, 2021.

[17] D. Tanner, J. A. Fitzgerald, and B. R. Phillips, "The kevlar story—an advanced materials case study," *Angewandte Chemie International Edition in English*, vol. 28, no. 5, pp. 649–654, 1989.

[18] B.-H. Lee, H.-J. Kim, and W.-R. Yu, "Fabrication of long and discontinuous natural fiber reinforced polypropylene biocomposites and their mechanical properties," *Fibers and Polymers*, vol. 10, no. 1, pp. 83–90, 2009.

[19] F. Ahmad, H. S. Choi, and M. K. Park, "A review: Natural fiber composites selection in view of mechanical, light weight, and economic properties," *Macromolecular materials and engineering*, vol. 300, no. 1, pp. 10–24, 2015.

[20] K. K. Chawla, "Carbon fiber composites," in *Composite Materials*, Springer, 1998, pp. 252–277.

[21] A. K. Sinha, H. K. Narang, and S. Bhattacharya, "Mechanical properties of natural fibre polymer composites," *Journal of Polymer Engineering*, vol. 37, no. 9, pp. 879–895, 2017. DOI: doi:10.1515/polyeng-2016-0362. [Online]. Available: https://doi.org/10.1515/polyeng-2016-0362.

[22] B. V. Ramnath, V. Manickavasagam, C. Elanchezhian, C. V. Krishna, S. Karthik, and K. Saravanan, "Determination of mechanical properties of intra-layer abaca–jute–glass fiber reinforced composite," *Materials & Design*, vol. 60, pp. 643–652, 2014.

[23] C. Subramanian and S. Senthilvelan, "Joint performance of the glass fiber reinforced polypropylene leaf spring," *Composite structures*, vol. 93, no. 2, pp. 759–766, 2011.

[24] J. Li, "The effect of surface modification with nitric acid on the mechanical and tribological properties of carbon fiber-reinforced thermoplastic polyimide composite," *Surface and Interface Analysis: An International Journal devoted to the development and application of techniques for the analysis of surfaces, interfaces and thin films*, vol. 41, no. 9, pp. 759–763, 2009.

[25] C. Sellitti, J. Koenig, and H. Ishida, "Surface characterization of graphitized carbon fibers by attenuated total reflection fourier transform infrared spectroscopy," *Carbon*, vol. 28, no. 1, pp. 221–228, 1990.

[26] T. Ohsawa, M. Miwa, M. Kawade, and E. Tsushima, "Axial compressive strength of carbon fiber," *Journal of applied polymer science*, vol. 39, no. 8, pp. 1733–1743, 1990.

[27] S. D. Shelare, R. Kumar, and P. B. Khope, "Flywheel energy application in commercial and agricultural field: A typical review," in *Recent Trends in Engineering Design*, Springer, 2021, pp. 177–186.

[28] N. Saha, A. N. Banerjee, and B. Mitra, "Dynamic mechanical study on unidirectional polyethylene fibers-pmma and glass fibers-pmma composite laminates," *Journal of applied polymer science*, vol. 60, no. 5, pp. 657–662, 1996.

[29] C. Pavlatos and V. Vita, "Linguistic representation of power system signals," in *Electricity Distribution*, Springer, 2016, pp. 285–295.

[30] M. Adhikari, "Natural fibre composites for injection moulding," pp. 1–96, 2012.

[31] A. Shahzad, "Hemp fiber and its composites - A review," *Journal of Composite Materials*, vol. 46, no. 8, pp. 973–986, 2012, ISSN: 00219983. DOI: 10.1177/0021998311413623.

[32] S. T. Peters, *Handbook of composites*. Springer Science & Business Media, 2013.

[33] T. Gutowski, "Advanced composites manufacturing john wiley & sons," *Inc. New York*, 1997.

[34] P. Monaghan, M. Brogan, and P. Oosthuizen, "Heat transfer in an autoclave for processing thermoplastic composites," *Composites Manufacturing*, vol. 2, no. 3-4, pp. 233–242, 1991.

[35] H. N. Dhakal and S. O. Ismail, "4 - design, manufacturing processes and their effects on bio-composite properties," in *Sustainable Composites for Lightweight Applications*, ser. Woodhead Publishing Series in Composites Science and Engineering, H. N. Dhakal and S. O. Ismail, Eds., Woodhead Publishing, 2021, pp. 121–177, ISBN: 978-0-12-818316-8. DOI: https://doi.org/10.1016/B978-0-12-818316-8.00005-0. [Online]. Available: https://www.sciencedirect.com/science/article/pii/B9780128183168000050.

[36] C. Tucker, *Injection and compression molding fundamentals, isayev, ai, ed. 481 (1987)*.

[37] S. Edebali, "15 - methods of engineering of biopolymers and biocomposites," in *Advanced Green Materials*, ser. Woodhead Publishing in Materials, S. Ahmed, Ed., Woodhead Publishing, 2021, pp. 351–357, ISBN: 978-0-12-819988-6. DOI: https://doi.org/10.1016/B978-0-12-819988-6.00015-X. [Online]. Available: https://www.sciencedirect.com/science/article/pii/B978012819988600015X.

[38] T. Manley, *Handbook of pultrusion technology: Rw meyer chapman and hall, new york and london, 1985, xii+ 180 pages,£ 32 isbn 0-412-00761-4*, 1987.

[39] S. Wiedmer, "Zur pultrusion von thermoplastischen halbzeugen: Prozessanalys und modelllbildung," 2006.

5

[40] S.-J. Liu, "Injection molding in polymer matrix composites," *Manufacturing Techniques for Polymer Matrix Composites (PMCs)*, pp. 15–46, 2012. DOI: 10.1533/9780857096258.1.13.

[41] M. Baum and D. Anders, "A numerical simulation study of mold filling in the injection molding process," *Computer Methods in Material Science*, vol. 21, no. 1, pp. 25–34, 2021, ISSN: 1641-8581. DOI: 10.7494/cmms.2021.1.0743.

[42] P. Kennedy and R. Zheng, *Flow analysis of injection molds: Second edition*. 2013, pp. 1–349, ISBN: 9781569905128. DOI: 10.3139/9781569905227.

[43] R. von Turkovich and L. Erwin, "Fiber fracture in reinforced thermoplastic processing," *Polymer Engineering & Science*, vol. 23, no. 13, pp. 743–749, 1983, ISSN: 15482634. DOI: 10.1002/pen.760231309.

[44] S. Patcharaphun and G. Opaskornkul, "Characterization of fiber length distribution in short andlong-glass-fiber reinforced polypropylene during injection molding process," *Agriculture and Natural Resources*, vol. 42, no. 5, pp. 392–397, 2008.

[45] A. Vaxman, M. Narkis, A. Siegmann, and S. Kenig, "Short-fiber thermoplastics composites: Fiber fracture during melt processing," *Wiley Encyclopedia of Composites*, pp. 1–19, 2011.

[46] U. Yilmazer and M. Cansever, "Effects of processing conditions on the fiber length distribution and mechanical properties of glass fiber reinforced nylon-6," *Polymer composites*, vol. 23, no. 1, pp. 61–71, 2002.

[47] J. Wang, C. Geng, F. Luo, *et al.*, "Shear induced fiber orientation, fiber breakage and matrix molecular orientation in long glass fiber reinforced polypropylene composites," *Materials Science and Engineering: A*, vol. 528, no. 7-8, pp. 3169–3176, 2011.

[48] G. Zhang and M. Thompson, "Reduced fibre breakage in a glass-fibre reinforced thermoplastic through foaming," *Composites Science and Technology*, vol. 65, no. 14, pp. 2240–2249, 2005.

[49] G. Stelzer, "Zum faser-und eigenschaftsabbau bei verarbeitung und recycling diskontinuierlich faserverstärkter kunststoffe: Anwendung des mikrobiegeversuchs zur faserfestigkeitsbestimmung am beispiel methodischer untersuchungen des eigenschaftsabbaus...," Ph.D. dissertation, Technische Universität Kaiserslautern, 2003.

[50] T. A. Osswald, "Understanding polymer processing," *Hanser: München, Germany*, 2010.

[51] A. Kelly and a. W. Tyson, "Tensile properties of fibre-reinforced metals: Copper/tungsten and copper/molybdenum," *Journal of the Mechanics and Physics of Solids*, vol. 13, no. 6, pp. 329–350, 1965.

[52] M. Rohde-Tibitanzl, "State of the art," in *Direct Processing of Long Fiber Reinforced Thermoplastic Composites and their Mechanical Behavior under Static and Dynamic Load*, pp. 3–68. DOI: 10.3139/9781569906309.002. eprint: https://www.hanser-elibrary.com/doi/pdf/10.3139/9781569906309.002. [Online]. Available: https://www.hanser-elibrary.com/doi/abs/10.3139/9781569906309.002.

5

[53] J. H. Phelps, A. I. Abd El-Rahman, V. Kunc, and C. L. Tucker III, "A model for fiber length attrition in injection-molded long-fiber composites," *Composites Part A: Applied Science and Manufacturing*, vol. 51, pp. 11–21, 2013.

[54] A. Durin, P. De Micheli, J. Ville, F. Inceoglu, R. Valette, and B. Vergnes, "A matricial approach of fibre breakage in twin-screw extrusion of glass fibres reinforced thermoplastics," *Composites Part A: Applied Science and Manufacturing*, vol. 48, no. 1, pp. 47–56, 2013, ISSN: 1359835X. DOI: 10.1016/j.compositesa.2012.12.011. [Online]. Available: http://dx.doi.org/10.1016/j.compositesa.2012.12.011.

[55] J. Kang, M. Huang, M. Zhang, *et al.*, "An effective model for fiber breakage prediction of injection-molded long fiber reinforced thermoplastics," *Journal of Reinforced Plastics and Composites*, vol. 39, no. 11-12, pp. 473–484, 2020, ISSN: 15307964. DOI: 10.1177/0731684420915643.

[56] V. B. Gupta, R. K. Mittal, P. K. Sharma, G. Mennig, and J. Wolters, "Some studies on glass fiber-reinforced polypropylene. Part I: Reduction in fiber length during processing," *Polymer Composites*, vol. 10, no. 1, pp. 8–15, 1989. DOI: 10.1002/pc.750100103.

[57] O. L. Forgacs and S. G. Mason, "Particle motions in sheared suspensions. IX. Spin and deformation of threadlike particles," *Journal of Colloid Science*, vol. 14, no. 5, pp. 457–472, 1959. DOI: 10.1016/0095-8522(59)90012-1.

[58] K. Albrecht, T. Osswald, E. Baur, T. Meier, S. Wartzack, and J. Müssig, "Fibre length reduction in natural fibre-reinforced polymers during compounding and injection moulding—experiments versus numerical prediction of fibre breakage," *Journal of Composites Science*, vol. 2, no. 2, 2018, ISSN: 2504477X. DOI: 10.3390/jcs2020020.

[59] A. Bechara, S. Goris, A. Yanev, D. Brands, and T. Osswald, "Novel modeling approach for fiber breakage during molding of long fiber-reinforced thermoplastics," *Physics of Fluids*, vol. 33, no. 7, 1ENG, 2021, ISSN: 10897666. DOI: 10.1063/5.0058693.

[60] T. Sasayama, M. Inagaki, and N. Sato, "Direct simulation of glass fiber breakage in simple shear flow considering fiber-fiber interaction," *Composites Part A: Applied Science and Manufacturing*, vol. 124, no. June, 2019, ISSN: 1359835X. DOI: 10.1016/j.compositesa.2019.105514.

[61] S. Goris, T. Back, A. Yanev, D. Brands, D. Drummer, and T. A. Osswald, "A novel fiber length measurement technique for discontinuous fiber-reinforced composites: A comparative study with existing methods," *Polymer Composites*, vol. 39, no. 11, pp. 4058–4070, 2018.

[62] C.-T. Huang and H.-C. Tseng, "Simulation prediction of the fiber breakage history in regular and barrier structure screws in injection molding," *Polymer Engineering & Science*, vol. 58, no. 4, pp. 452–459, 2018.

[63] A. Inoue, K. Morita, T. Tanaka, Y. Arao, and Y. Sawada, "Effect of screw design on fiber breakage and dispersion in injection-molded long glass-fiber-reinforced polypropylene," *Journal of Composite Materials*, vol. 49, no. 1, pp. 75–84, 2015.

[64] S. Simon, "Analysis of fiber attrition and fiber-matrix separation during injection molding of long fiberreinforced thermoplastic parts," Ph.D. dissertation, Master Thesis. Austrian Biotech University of Applied Sciences, 2016.

[65] F. Inceoglu, J. Ville, N. Ghamri, *et al.*, "Correlation between processing conditions and fiber breakage during compounding of glass fiber-reinforced polyamide," *Polymer Composites*, vol. 32, no. 11, pp. 1842–1850, 2011.

[66] P.-W. Huang, H.-S. Peng, S.-J. Hwang, and C.-T. Huang, "The low breaking fiber mechanism and its effect on the behavior of the melt flow of injection molded ultra-long glass fiber reinforced polypropylene composites," *Polymers*, vol. 13, no. 15, p. 2492, 2021.

[67] J. M. Burgers, "On the motion of small particles of elongated form suspended in a viscous liquid," *Kon. Ned. Akad. Wet. Verhand.(Eerste Sectie)*, vol. 16, pp. 113–184, 1938.

[68] K. Shon, D. Liu, and J. White, "Experimental studies and modeling of development of dispersion and fiber damage in continuous compounding," *International Polymer Processing*, vol. 20, no. 3, pp. 322–331, 2005.

[69] H. Chen, M. Cieslinski, and D. G. Baird, "Progress in modeling long glass and carbon fiber breakage during injection molding," *AIP Conference Proceedings*, vol. 1664, 2015, ISSN: 15517616. DOI: 10.1063/1.4918422.

[70] J. H. Phelps, *Processing-microstructure models for short-and long-fiber thermoplastic composites*. University of Illinois at Urbana-Champaign, 2009.

[71] Y. Masubuchi, M. Terada, A. Yamanaka, T. Yamamoto, and T. Ishikawa, "Distribution function of fiber length in thermoplastic composites," *Composites Science and Technology*, vol. 134, pp. 43–48, 2016, ISSN: 0266-3538. DOI: https://doi.org/10.1016/j.compscitech.2016.08.007. [Online]. Available: https://www.sciencedirect.com/science/article/pii/S0266353816309009.

[72] D. Huang and X. Zhao, "Novel modified distribution functions of fiber length in fiber reinforced thermoplastics," *Composites Science and Technology*, vol. 182, p. 107 749, 2019.

[73] T. C. Chang, A. B. Senior, H. Celik, D. Brands, A. Yanev, and T. Osswald, "Validation of fiber breakage in simple shear flow with direct fiber simulation," *Journal of Composites Science*, vol. 4, no. 3, 2020, ISSN: 2504477X. DOI: 10.3390/jcs4030134.

[74] O. Das, N. Kim, and D. Bhattacharyya, "16 - the mechanics of biocomposites," in *Biomedical Composites (Second Edition)*, ser. Woodhead Publishing Series in Biomaterials, L. Ambrosio, Ed., Second Edition, Woodhead Publishing, 2017, pp. 375–411, ISBN: 978-0-08-100752-5. DOI: https://doi.org/10.1016/B978-0-08-100752-5.00017-2. [Online]. Available: https://www.sciencedirect.com/science/article/pii/B9780081007525000172.

5

[75] P. Mallick, "Chapter 5 - thermoplastics and thermoplastic–matrix composites for lightweight automotive structures," in *Materials, Design and Manufacturing for Lightweight Vehicles (Second Edition)*, ser. Woodhead Publishing in Materials, P. Mallick, Ed., Second Edition, Woodhead Publishing, 2021, pp. 187–228, ISBN: 978-0-12-818712-8. DOI: https://doi.org/10.1016/B978-0-12-818712-8.00005-7. [Online]. Available: https://www.sciencedirect.com/science/article/pii/B9780128187128000057.

[76] G. H. Staab, "1 - introduction to composite materials," in *Laminar Composites*, G. H. Staab, Ed., Woburn: Butterworth-Heinemann, 1999, pp. 1–16, ISBN: 978-0-7506-7124-8. DOI: https://doi.org/10.1016/B978-075067124-8/50001-1. [Online]. Available: https://www.sciencedirect.com/science/article/pii/B9780750671248500011.

[77] M. Cordin, T. Bechtold, and T. Pham, "Effect of fibre orientation on the mechanical properties of polypropylene–lyocell composites," *Cellulose*, vol. 25, no. 12, pp. 7197–7210, 2018.

[78] H. V. Patel and H. K. Dave, "Effect of fiber orientation on tensile strength of thin composites," *Materials Today: Proceedings*, vol. 46, pp. 8634–8638, 2021.

[79] J. H. S. Almeida Jr, C. C. Angrizani, E. C. Botelho, and S. C. Amico, "Effect of fiber orientation on the shear behavior of glass fiber/epoxy composites," *Materials & Design (1980-2015)*, vol. 65, pp. 789–795, 2015.

[80] S. Mortazavian and A. Fatemi, "Effects of fiber orientation and anisotropy on tensile strength and elastic modulus of short fiber reinforced polymer composites," *Composites part B: engineering*, vol. 72, pp. 116–129, 2015.

[81] H. Wang, H. Zhou, L. Gui, H. Ji, and X. Zhang, "Analysis of effect of fiber orientation on young's modulus for unidirectional fiber reinforced composites," *Composites part B: engineering*, vol. 56, pp. 733–739, 2014.

[82] A. B. Senior and T. Osswald, "Measuring fiber length in the core and shell regions of injection molded long fiber-reinforced thermoplastic plaques," *Journal of Composites Science*, vol. 4, no. 3, 2020, ISSN: 2504-477X. DOI: 10.3390/jcs4030104. [Online]. Available: https://www.mdpi.com/2504-477X/4/3/104.

[83] A. Bechara, "Modeling fiber damage during processing of long fiber-reinforced thermoplastic composites," 2021.

A

PHELPS MODEL VALIDATION

This section will perform the validation of the Phelps model developed in the MATLAB code for a single point by comparing it to the results obtained in the literature ([70]).

The Phelps model created for the analytical evaluation as a post-processor to the input data needs to be verified to ascertain its accuracy. This is done by replicating the case of the fiber length degradation observed in a homogeneous simple shear flow, as observed in the section 5.4 of [53]. An initial condition of the 1000 randomly oriented fibers, each with an initial fiber length of 6 mm is considered. The physical parameters considered include a simple shear flow with shear rate ($\dot{\gamma}$) = 500 s^{-1}, the fiber modulus (E_f) = 73 GPa, fiber diameter (d_f) = 17 μm and matrix viscosity (η_m) = 1000 Pa.s. The resolution for the discrete fiber length is chosen as (Δl) = 100 μm ($l_{max} = 6mm, M = 60$), and the Phelps model parameters to be: $\zeta = 3, C_B = 2 * 10^{-3}$ and $S = 0.25$. With the flow conditions, material properties and the model constants defined, the simulation was created using the relevant equations. First, P_i was calculated using Equation A.1 and then fiber length distribution was calculated using Equation A.2 and Equation A.3 each time steps. The simulation was run for a period of 6 seconds, and the fiber length distribution was estimated at four different times. The equations are also presented here for convenience:

$$P_i = \begin{cases} 0 & \text{for} \quad B_i < 1 \\ C_B \dot{\gamma} \left[1 - \exp\left(1 - B_i\right)\right] & \text{for} \quad B_i \geqslant 1 \end{cases} \tag{A.1}$$

$$N_{i,j+1} = N_{i,j} - P_i N_{i,j} \Delta t + \sum_{k|k \geq i}^{M} R_{ik} N_{k,j} \Delta t \tag{A.2}$$

$$R_{ik} = \alpha_k N_{\text{PDF}} \left(i\Delta l, \frac{k\Delta l}{2}, Sk\Delta l \right) \tag{A.3}$$

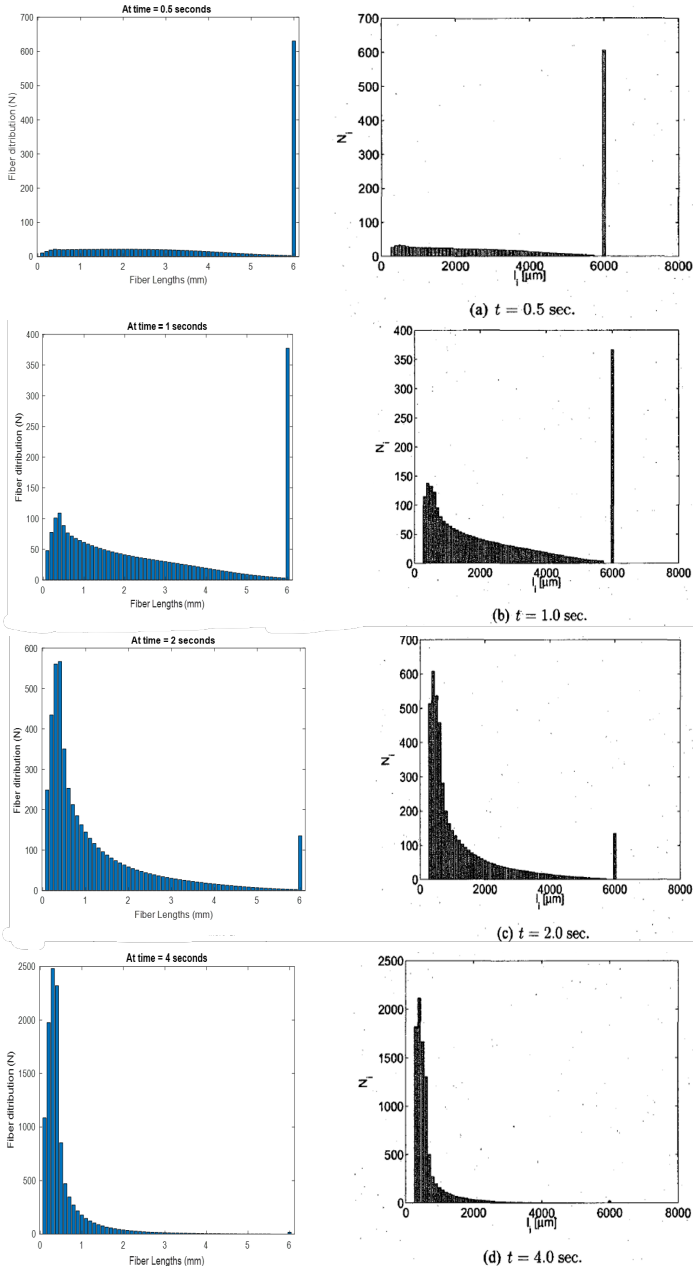

Figure A.1: Fiber length distributions presented at (a) 0.5 seconds (b) 1 second (c) 2 seconds and (d) 4 seconds.

From the results, it is apparent that the agreement is quite strong, which validates the fact that fiber length evolution model developed in this study.

Further, to completely validate the model, the total conservation of fiber length needs to be satisfied. This means that the sum of all fiber lengths should remain the same before and after the breakage,

$$L_{\text{total}} = \sum N_i l_i \tag{A.4}$$

or it can be implied that Equation A.4 should remain constant with time. T

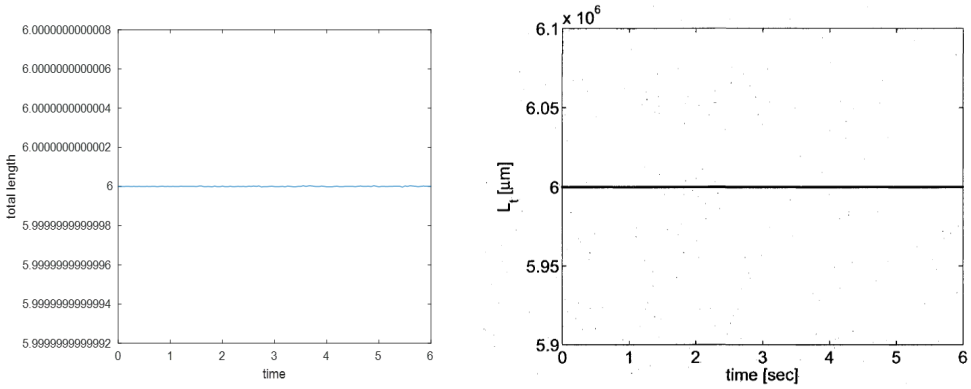

Figure A.2: Change of total fiber lengths over time. A constant line implies that the fiber length is conserved.

From the plot (Figure A.2), it can be again observed that the total fiber length is conserved. Therefore, with all the results obtained as of now, it can be claimed that the model has been replicated quite well.

B

BECHARA MODEL VALIDATION

This section will perform the validation of the Bechara model developed in the MATLAB code, by comparing it to the results obtained for the model in the literature ([83]).

To perform the development of the Becahara model in the MATLAB, it is first needed to develop an understanding of the model by replicating the work performed in the literature ([83]). The method developed to perform the replication, along with the flow and material properties assumed are further explained.

First a set of experimental results are obtained from a set of couette rheometer experiments performed during the research. In the experiments, the fiber lengths were recorded after shearing was allowed in the experiments for different residence times. These results are also showed in the Table B.1.

Table B.1: Averaged fiber lengths measured for fiber length evolution with different residence time in the literature [59]

Time	Weight average fiber lengths (L_w) in mm	Number average fiber lengths (L_n) in mm
0	15	15
30	3.75	1.22
45	2.45	0.94
60	1.81	0.72
90	1.34	0.63
120	1.22	0.61
300	1.42	0.67

The model was then employed to match the trend observed in the experiment, by using the appropriate fitting parameters. Apart from the fitting parameters, material properties and the flow rheology properties also need to be established. The material used in the study is glass fiber reinforced thermoplastic polymer with 30% fiber concentration by weight. The flow properties for the experiments, as proposed in the literature are ($\dot{\gamma}$) = 58.64 s^{-1} and matrix viscosity (η_m) = 135.38 Pa.s. The residence time for the experiment is set to 300 seconds and the initial fiber length is 15 mm.

With the relevant properties established, the model is then applied through the number averaged and weight averaged fiber length evolution equations, which have been

explained in subsection 3.3.2 and have been placed here as well for reference.

$$\frac{dL_N}{dt} = -k_{N,f}\left(L_N - L_{N,\infty}\right) \tag{B.1}$$

$$\frac{dL_W}{dt} = -k_{W,f}\left(L_W - L_{W,\infty}\right) \tag{B.2}$$

$$L_\infty = \lambda\left(\frac{\sigma_u d_f^2}{\eta_m \dot{\gamma}}\right)^{1/2} \tag{B.3}$$

$$k_f = \xi\dot{\gamma} \tag{B.4}$$

The fitting parameters, k_f and λ have been taken from the paper as well, and presented in the Table B.2 along with other material and rheology properties.

Table B.2: Input fiber material properties, flow conditions and model fitting parameters to perform the validation of the Bechara model with the literature [59].

Initial fiber length	15 mm
Fiber ultimate strength	2.6 GPa
Residual time	15 s
Shear rate	58.64 s^{-1}
viscosity	135.38 Pa.S
Material fitting parameter	0.085
ξ Pre-dispersion for L_w	1.21×10^{-3}
ξ Post-dispersion for L_w	4.66×10^{-4}
ξ Pre-dispersion for L_n	1.45×10^{-3}
ξ Post dispersion for L_n	4.97×10^{-4}

From the Table B.2, it can be observed that tere are two ξ factors for both types of averaged lengths, one pre-dispersion, and one post-dispersion. This is used to fit the experimental much better, as the fibers in the initial stage of breakage have higher tendency to break due to more fiber interactions. However, with time, this tendency decreases, and therefore, fiber breakage rate also changes. Based on the above equations and given fitting parameters and properties, the model was applied in the MATLAB code, and the following results were obtained.

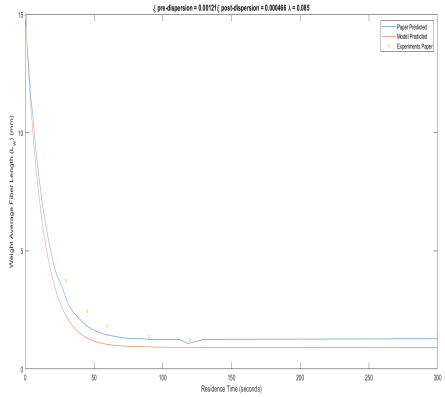

(a)

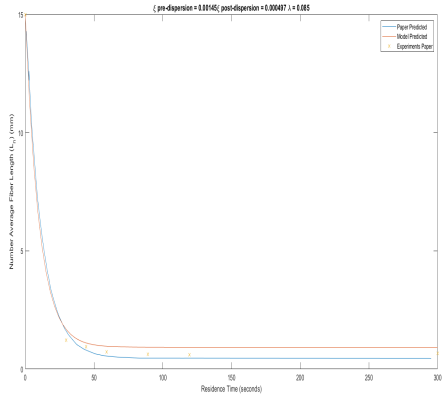

(b)

Figure B.1: (a) Weight averaged fiber length evolution (L_w) (b) Number averaged fiber length evolution (L_n) comparison as obtained from the the literature ([59]) and the MATLAB analytical model for validation.

From the Figure B.1, it can be observed that the fiber lengths evolution is predicted quite well by the model applied in the MATLAB. It slightly under predicts as compared to the experimental data used, in case of L_w, which is also observed in the paper prediction, However, in the case of L_n, there is slight over prediction observed in case of the residual lengths. This is perhaps attributed to the values of the fitting parameters used, which are slightly approximated, due to unavailability of the complete data in the literature. However, the overall agreement between the trends is quite acceptable, and therefore, it can be claimed that the model has been replicated quite well.

C

Mesh Convergence Study

This part of the appendix performs a mesh convergence study.

To estimate the convergence of the mesh element size, a simple beam geometry was input into the Moldex3D software. To collect the data, 3 measure nodes were inserted at 3 different cross sections, as shown in Figure C.1. Further, Figure C.2 presents the meshes at these cross-sections for different mesh sizes for BLM and eDesign modes.

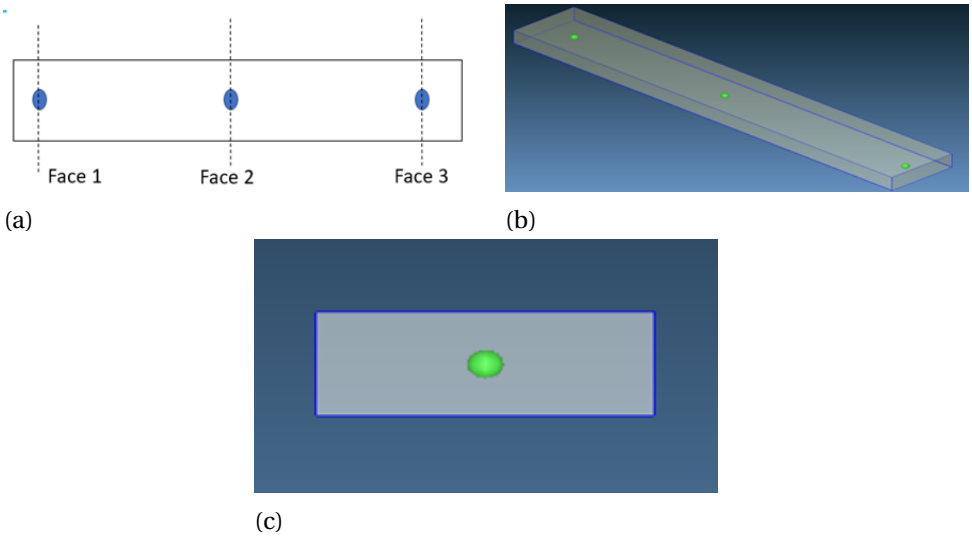

Figure C.1: (a) Schematic of the beam indicating the faces considered to measure fiber length. (b) Isometric view of the model with actual measure nodes. (c) Front view of the cross section of the model with measure node.

Table C.1: Input computational parameters for the mesh convergence study.

Fiber diameter (μm)	Fiber aspect ratio	Weight %	S	C_B	ζ
12	312.5	30	1	0.03	0.55

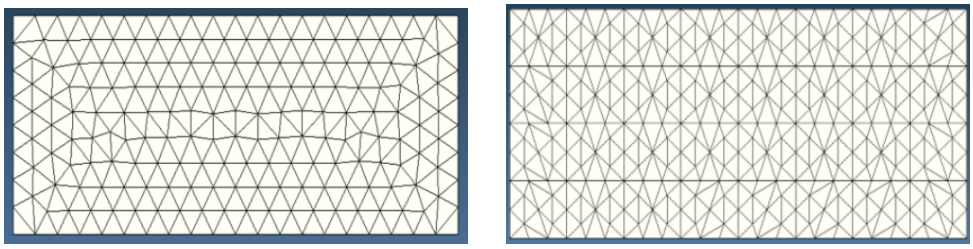

(a) (b)

Figure C.2: Cross sectional view of meshes generated (a) with BLM mesh size 0.5 mm and (b) with eDesign mesh size 0.5 mm.

While performing the convergence, a set of input data was selected at random, but was kept constant with different trial runs, as the primary objective is to check the influence of mesh size on results. These input are represented in the Table C.1. The results represent the fiber lengths obtained at these sections, as in this work, fiber attrition in injection molding is the main objective.

The results obtained for the convergence of these meshes are presented in the Figure C.3. The converging element size is selected where the curve begins to flatten (in the Figure C.3) and the difference in fiber lengths between succeeding mesh sizes diminish. For the BLM mesh, the convergence happens for mesh sizes 1 mm and smaller, and for eDesign, it happens for mesh sizes 0.5 mm and smaller. Based on these results, the element size of 0.5 mm is selected as the default element size for the meshing of the mold cavity insert to be used for experimental simulations.

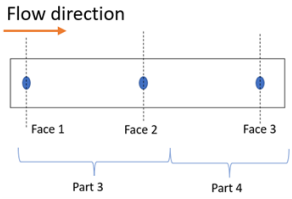

(a)

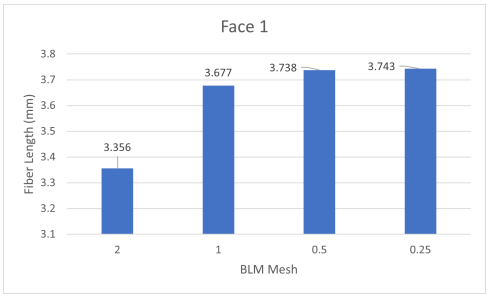

(b)

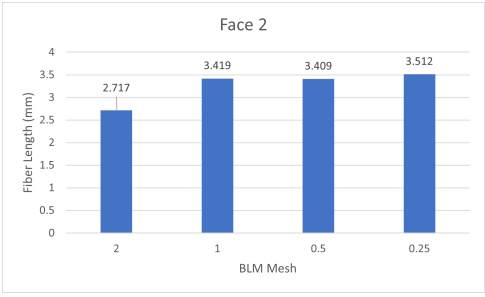

(c)

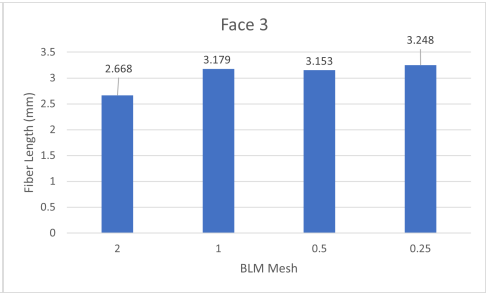

(d)

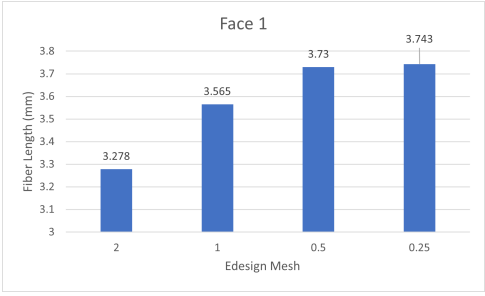

(e)

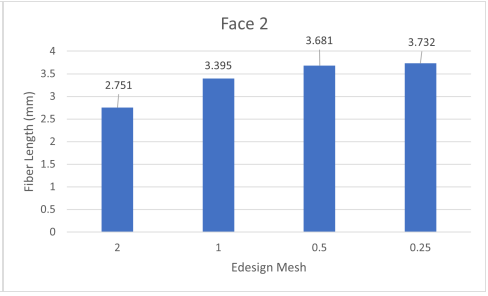

(f)

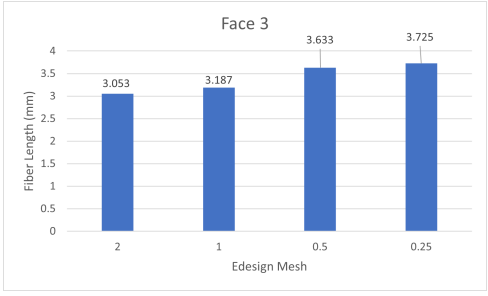

(g)

Figure C.3: Mesh geometry schematic used with flow direction presented in (a).Meshing convergence observed for BLM meshes with different sizes at faces: (b) Face 1,(c) Face 2 & (d) Face 3; And for eDesign mesh:(e) Face 1,(f) Face 2 & (g) Face 3